Prostaglandins temporally regulate cytoplasmic actin bundle formation during *Drosophila* oogenesis

Andrew J. Spracklen[a], Daniel J. Kelpsch[a], Xiang Chen[a], Cassandra N. Spracklen[b], and Tina L. Tootle[a]

[a]Anatomy and Cell Biology, Carver College of Medicine and [b]Department of Epidemiology, College of Public Health, University of Iowa, Iowa City, IA 52242

ABSTRACT **Prostaglandins (PGs)—lipid signals produced downstream of cyclooxygenase (COX) enzymes—regulate actin dynamics in cell culture and platelets, but their roles during development are largely unknown. Here we define a new role for Pxt, the *Drosophila* COX-like enzyme, in regulating the actin cytoskeleton—temporal restriction of actin remodeling during oogenesis. PGs are required for actin filament bundle formation during stage 10B (S10B). In addition, loss of Pxt results in extensive early actin remodeling, including actin filaments and aggregates, within the posterior nurse cells of S9 follicles; wild-type follicles exhibit similar structures at a low frequency. Hu li tai shao (Hts-RC) and Villin (Quail), an actin bundler, localize to all early actin structures, whereas Enabled (Ena), an actin elongation factor, preferentially localizes to those in *pxt* mutants. Reduced Ena levels strongly suppress early actin remodeling in *pxt* mutants. Furthermore, loss of Pxt results in reduced Ena localization to the sites of bundle formation during S10B. Together these data lead to a model in which PGs temporally regulate actin remodeling during *Drosophila* oogenesis by controlling Ena localization/activity, such that in S9, PG signaling inhibits, whereas at S10B, it promotes Ena-dependent actin remodeling.**

Monitoring Editor
Jeffrey D. Hardin
University of Wisconsin

Received: Jul 5, 2013
Revised: Oct 24, 2013
Accepted: Nov 20, 2013

INTRODUCTION

Development and adult tissue homeostasis require dramatic movements and reorganization of both cells and whole tissues. Underlying all of these processes is the actin cytoskeleton, which serves as a dynamic scaffold to facilitate cell migration, cell division, and cell shape. Tight regulation of actin cytoskeletal dynamics is mediated by the concerted activity of >100 known actin-binding proteins (reviewed in Pollard and Borisy, 2003). Although much is known about how the activity of individual actin-binding proteins are regulated, very little is known about the mechanisms by which the activity of multiple actin-binding proteins is coordinated to mediate developmental processes and tissue homeostasis.

One possible mechanism by which such coordination may occur is through prostaglandin (PG) signaling. PGs are small, bioactive lipids that act as paracrine and autocrine signaling molecules to regulate numerous physiological processes, including pain, inflammation, fertility, and cardiovascular function (reviewed in Tootle, 2013). PGs are synthesized downstream of cyclooxygenase enzymes (COX1 and COX2), which convert free arachidonic acid into the precursor PGH_2, and are the pharmacologic targets of nonsteroidal anti-inflammatory drugs. PGH_2 is then processed into biologically active prostanoids (including PGD_2, PGE_2, $PGF_{2\alpha}$, PGI_2, and thromboxane A_2 [TXA_2]) downstream of COX enzymes through the activity of specific synthases (PGD_2: H-PGDS and L-PGDS; PGE_2: mPGES-1, mPGES-2, and cPGES; $PGF_{2\alpha}$: AKR1B1; PGI_2: PGIS; and TXA_2: TXAS). After their synthesis, PGs most commonly serve as ligands for specific G protein–coupled receptors (Hirata *et al.*, 1991; PGD_2: DP and CRTH2; PGE_2: EP1, EP2, EP3, and EP4; $PGF_{2\alpha}$: FP;

This article was published online ahead of print in MBoC in Press (http://www.molbiolcell.org/cgi/doi/10.1091/mbc.E13-07-0366) November 27, 2013.

Address correspondence to: Tina L. Tootle (tina-tootle@uiowa.edu).

Abbreviations used: AG, aberrant actin aggregate structure; COX, cyclooxygenase; EF, extensive, early actin filament; Ena, Enabled; Evl, Ena/VASP-like; F-actin, filamentous actin; Hts-RC, Hu li tai shao-ring canal–specific isoform; Mena, mammalian Ena; PG, prostaglandin; PKA, protein kinase A; VASP, vasodilator-stimulated phosphoprotein.

and PGI_2: IP), which elicit their downstream effects through activation of Gα and, in some cases, Gβγ (Speirs *et al.*, 2010). In addition, PGs may induce mitogen-activated protein kinase signaling pathways, activate Rho GTPases, or serve as PPARγ nuclear hormone receptor ligands (reviewed in Bos *et al.*, 2004).

In vitro studies provide evidence that PG signaling can regulate the actin cytoskeleton in both a cell-type– and a PG-type–dependent manner. For example, TXA_2 and $PGF_{2\alpha}$ stimulate actomyosin-based contractility, whereas PGE_2 and PGI_2 promote relaxation in hepatic stellate cells (Kawada *et al.*, 1992). Subsequently, PGs were found to have opposing effects on cytoplasmic actin filaments (i.e., actin stress fibers) in multiple cell types. Whereas PGE_2 promotes actin stress fiber assembly in rat inner medullary collecting duct cells (Tamma *et al.*, 2003) and stability in IEC-6 cells (Banan *et al.*, 2000), it induces actin stress fiber disassembly in A431 cells, HeLa cells, rat-1 fibroblasts (Peppelenbosch *et al.*, 1993), and human aortic smooth muscle cells (Bulin *et al.*, 2005). Similarly, both PGE_2 and PGI_2 promote actin stress fiber disassembly in human pulmonary artery endothelial cells (Birukova *et al.*, 2007). $PGF_{2\alpha}$ promotes filopodia retraction and actin stress fiber assembly in 293-EBNA cells (Pierce *et al.*, 1999). In human umbilical vein endothelial cells, TXA_2 slows $\alpha_v\beta_3$-dependent cell adhesion and inhibits cell spreading, whereas PGE_2 accelerates cell adhesion and promotes cell spreading (Dormond *et al.*, 2002). Of interest, cytoskeletal inputs (i.e., mechanical stretching) have been shown to induce COX2-dependent production of PGE_2, which subsequently leads to disassembly of actin stress fibers in murine podocytes (Martineau *et al.*, 2004).

PG signaling is also known to directly regulate platelet activation and aggregation, which requires actin cytoskeletal remodeling, including the rapid generation of filopodia that mediate protrusion and adhesion (reviewed in Bearer *et al.*, 2002). TXA_2, the major prostanoid produced in human platelets, is a potent activator of platelet aggregation (Hamberg *et al.*, 1975), whereas PGI_2 (Moncada *et al.*, 1977), PGE_1 (Kloeze, 1966), and PGD_2 (Smith *et al.*, 1974) inhibit platelet aggregation. In addition, PGE_2 has been shown to both potentiate (Kloeze, 1966; Willis, 1974) and inhibit platelet aggregation (Smith *et al.*, 2010; Petrucci *et al.*, 2011).

The aforementioned studies provided some insight into the mechanisms by which PGs regulate cytoplasmic actin filament remodeling. Multiple in vitro studies demonstrate that the PG-dependent morphological changes in cytoplasmic actin bundles occur via cAMP-dependent mechanisms, albeit through different downstream events, including cAMP-dependent kinase (protein kinase A [PKA]) and nucleotide exchange proteins directly activated by cAMP (Epac1)/Ras-related protein 1 (Rap1)–dependent activation of Rac (Birukova *et al.*, 2007), PKA-dependent Rac activation and Rac-independent activities (Dormond *et al.*, 2002), and PKA-dependent decreases in focal adhesion kinase phosphorylation (Bulin *et al.*, 2005). Other in vitro studies implicate Rho activation downstream of PGs in driving the changes in actin stress fiber assembly (Pierce *et al.*, 1999; Tamma *et al.*, 2003). Furthermore, PGI_2 (Nolte *et al.*, 1991) and PGE_1 (Halbrugge *et al.*, 1990; Nolte *et al.*, 1991) block platelet activation through cAMP/cGMP-dependent phosphorylation of vasodilator-stimulated phosphoprotein (VASP), a member of the Enabled (Ena)/VASP family of actin elongation factors (Aszodi *et al.*, 1999; Bearer *et al.*, 2000). Thus, although these studies provided some insight into the mechanisms by which PG signaling regulates cytoplasmic actin filament assembly/disassembly, much remains to be determined, including how multiple PG signals are integrated to coordinate actin remodeling and the mechanisms through which particular PG signals regulate actin dynamics. Previously we established *Drosophila* oogenesis as a model with which to begin to address these questions (Tootle and Spradling, 2008).

Drosophila oogenesis is a well-established model system for studying actin cytoskeletal remodeling and regulation (reviewed in Hudson and Cooley, 2002). It consists of 14 well-characterized, morphological stages of follicle development (reviewed in Spradling, 1993). At stage 9 (S9) of follicle development, the follicle consists of 16 germline-derived cells (15 support or nurse cells and a single oocyte), which are surrounded by ~1000 somatically derived epithelial cells (Figure 1A). Multiple processes occur during S9 that are critical for female fertility. A small group (six to eight) of cells, termed border cells, delaminate from the anterior of the follicle and migrate between the nurse cells toward the dorsal anterior of the oocyte, and the remaining follicle cells migrate posteriorly over the nurse cells and oocyte to form an anterior-posterior gradient of follicle cell thickness (Figure 1, A and B; reviewed in Montell *et al.*, 2012). During S9, the oocyte actively takes up yolk granules from the hemolymph (Bownes and Hames, 1978; Bownes and Hodson, 1980), and microtubule-dependent, slow cytoplasmic streaming establishes oocyte polarity (Gutzeit, 1986; Theurkauf *et al.*, 1992). Aside from cortical actin deposits, the cytoplasm of the nurse cells is largely devoid of actin filament bundles through the end of S10A. During S10B, the actin cytoskeleton within the nurse cells undergoes rapid remodeling, resulting in increased cortical actin deposition and formation of a cage-like network of parallel actin filament bundles extending from the nurse cell membranes inward, toward the nurse cell nuclei (Figure 1, A and E–E′; Guild *et al.*, 1997; Huelsmann *et al.*, 2013). This dramatic actin remodeling is required to provide the contractile force necessary for the rapid transfer of nurse cell cytoplasm (nurse cell dumping) into the growing oocyte at S11 (Wheatley *et al.*, 1995) while preventing the nurse cell nuclei from obstructing the ring canals—specialized cytoplasmic bridges—through which the cytoplasm must flow (Cooley *et al.*, 1992; Mahajan-Miklos and Cooley, 1994a).

Previously we identified critical roles for PG signaling in regulating actin bundle formation during S10B (Tootle and Spradling, 2008) and gene expression (Tootle *et al.*, 2011) during *Drosophila* oogenesis. Using this same model, we established Fascin, an actin-bundling protein, as a novel downstream target of PG signaling during PG-dependent actin remodeling during S10B (Groen *et al.*, 2012). Thus *Drosophila* oogenesis is an attractive model for identifying the likely conserved mechanisms by which PG signaling coordinates actin cytoskeletal remodeling.

Here we present our finding that PG signaling temporally regulates the onset of actin remodeling during *Drosophila* oogenesis. Whereas our prior studies largely focused on the cytoskeletal events occurring during S10B, here we primarily focus on the previously undescribed role of PGs in modulating actin filament formation during S9. Wild-type S9 follicles exhibit a low frequency of early actin structures in the posterior nurse cells, whereas loss of Pxt, the *Drosophila* COX-like enzyme, results in the highly penetrant presence of extensive actin filament and aggregate formation in the posterior nurse cells at S9. We find that two actin-binding proteins, Hu li tai shao-ring canal–specific isoform (Hts-RC) and Quail (Villin), localize to early actin structures in wild-type and *pxt* mutant S9 follicles, whereas Enabled (Ena), the sole Ena/VASP family member found in *Drosophila* (Gertler *et al.*, 1996), localizes preferentially to those early actin structures found in *pxt* mutants. Furthermore, genetic reduction of Ena in *pxt* mutants suppresses this early actin remodeling. In addition, we find that Ena localization to the sites of parallel actin filament bundle formation at S10B is reduced in *pxt* mutants. Together these data are consistent with a model in which PG signaling cascades regulate Ena

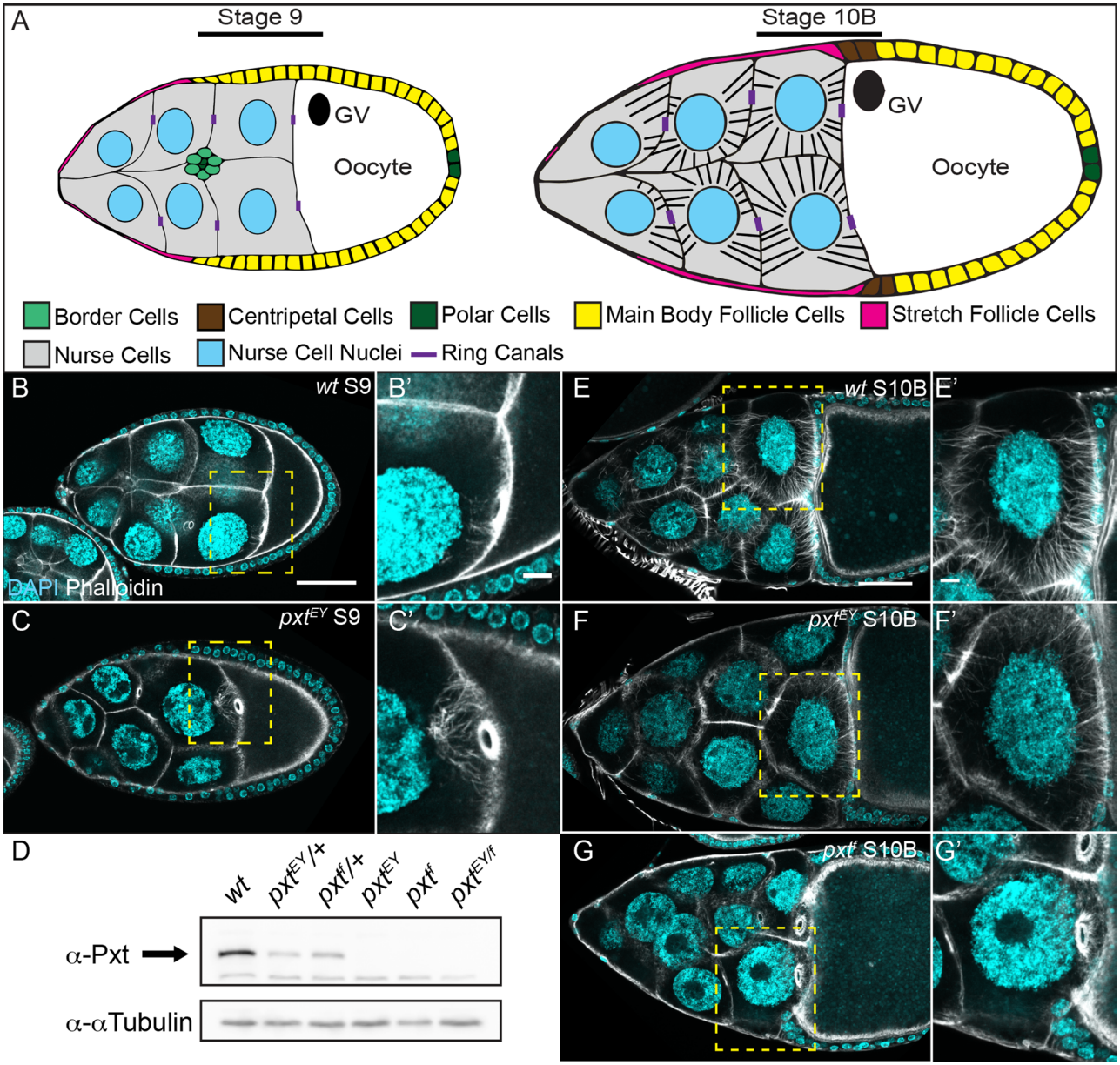

FIGURE 1: Pxt temporally regulates actin remodeling during mid-oogenesis. (A) Schematic detailing the cellular composition of S9 and S10B follicles; GV, germinal vesicle. (B–C′, E–G′) Maximum projections of confocal slices of follicles, staged as indicated, taken at 20× magnification. Anterior is to the left. F-actin (phalloidin), white; DNA (DAPI), cyan. (B–B′, E–E′) Wild type, wt (*yw*). (C–C′, F–F′) pxt^{EY}. (G–G′) pxt^{f}. (D) Representative Western blot for Pxt levels. S9 and S10B follicles consist of 16 germline-derived cells (one oocyte [white] and 15 nurse cells [gray]) surrounded by a somatic epithelium (A). In wild-type S9 follicles, the nurse cell cytoplasm is largely devoid of actin filament structures (B–B′). During S10B, wild-type follicles undergo actin remodeling to generate a network of parallel actin filament bundles extending from the nurse cell membranes toward the nuclei (E–E′). *pxt* mutants exhibit early actin remodeling, resulting in the formation of extensive early actin filaments and actin aggregates at S9 (C–C′ vs. B–B′). In addition, *pxt* mutants exhibit a range of actin-remodeling defects at S10B, ranging from mild defects in the number and distribution of actin filament bundles (F–F′) to near-complete loss of actin filament bundles (G–G′). Both pxt^{EY} and pxt^{f} homozygotes, as well as their heteroallelic combination, exhibit a substantial loss of Pxt protein (D). Images are representative and taken from multiple experiments. Scale bars, 50 μm (B–G), 10 μm (B′–G′).

localization/activity to temporally regulate actin filament formation during *Drosophila* oogenesis, at least in part by restricting Ena localization/activity earlier in oogenesis (S9) and promoting appropriate Ena localization/activity later in oogenesis (S10B). Further understanding of the mechanisms by which PGs exert opposing effects on Ena localization/activity during *Drosophila* oogenesis is likely to shed light on conserved mechanisms by which PGs may generally regulate the Ena/VASP family of proteins.

RESULTS

Prostaglandin signaling temporally regulates actin remodeling

Previously we showed that Pxt, the *Drosophila* COX1-like enzyme, is required for actin remodeling at S10B and subsequent female fertility (Tootle and Spradling, 2008; Groen *et al.*, 2012). Recently we observed that Pxt plays a key role in temporally regulating the onset of actin remodeling during mid-oogenesis, S9–10B (see *Materials*

and Methods for detailed staging information). Aside from cortical actin deposits underlying the nurse cell membranes, the nurse cells of wild-type S9 (Figure 1, B–B′) and S10A follicles are largely devoid of filamentous actin (F-actin) structures. However, *pxt* mutants exhibit early actin filament and actin aggregate structures in the four posterior nurse cells at S9 (Figure 1, C–C′), suggesting that perturbation of PG signaling disrupts temporal regulation of the onset of actin remodeling during *Drosophila* oogenesis.

During S10B, wild-type follicles undergo dramatic actin remodeling, resulting in strengthening of cortical actin deposits and the assembly of parallel actin filament bundles, which extend from the nurse cell membranes toward the nurse cell nuclei (Figure 1, E–E′; Guild *et al.*, 1997; Huelsmann *et al.*, 2013). Loss of Pxt results in a range of actin-remodeling defects during S10B, with the most severe phenotype, most often observed in pxt^{f01000} mutants (subsequently referred to as pxt^{f}), resulting in a complete loss of parallel actin filament bundle formation and cortical actin breakdown (Figure 1, G–G′). Less severe *pxt* mutant (pxt^{f}, $pxt^{EY03052}$ [pxt^{EY}], and $pxt^{EY03052/f01000}$ [$pxt^{EY/f}$]) phenotypes include reduced bundle formation and altered bundle length and distribution compared with wild type (Figure 1, F–F′ compared with E–E′). These data suggest that the pxt^{f} and pxt^{EY} alleles possess differential abilities to undergo canonical actin remodeling at S10B, with pxt^{EY} mutant being more capable of generating parallel actin filament bundles than pxt^{f} mutants (Tootle and Spradling, 2008; Groen *et al.*, 2012).

This allele-specific difference may be due to the nature of these alleles. The two alleles, both recovered from large-scale insertional mutagenesis screens, result from two distinct elements (pxt^{f}, a Piggybac insertion in the 5′ untranslated region and just upstream of the translation start site at +60; pxt^{EY}, a P-element insertion upstream of the transcription start site at −17) that seem to have differential effects on *pxt* mRNA levels. Although quantitative real-time PCR indicated that homozygosity for either allele resulted in a substantial reduction in *pxt* mRNA, in situ hybridization revealed that the alleles exhibit different expression patterns. Whereas the pxt^{f} ovaries exhibited a near-complete loss of *pxt* mRNA, pxt^{EY} ovaries exhibited a very low but uniform expression pattern (Tootle and Spradling, 2008). It is intriguing that in wild-type ovaries, *pxt* is expressed at low levels early in oogenesis but exhibits up-regulation beginning at S10A. To assess whether the alleles exhibit a differential effect on Pxt protein levels, we generated a polyclonal antibody using a purified peptide as the antigen. Based on Western blot analysis of whole-ovary lysates, both alleles exhibit a substantial, if not complete, loss of Pxt protein compared with wild type or *pxt* heterozygotes (Figure 1D and Supplemental Figure S1). This, however, does not completely exclude the possibility that pxt^{EY} mutants produce very low levels of Pxt protein, making them more capable of generating F-actin structures than pxt^{f} mutants.

Early actin remodeling is highly penetrant in *pxt* mutants

Wild-type S9 follicles typically possess minimal actin filament bundle structures emanating inward from the posterior ring canals of the four nurse cells adjacent to the oocyte, forming cone-like structures (Figure 2, A–B′ and E). Occasionally, the posterior nurse cells of wild-type S9 follicles undergo a more substantial actin remodeling, which we term "early actin remodeling," with 4% of S9 follicles exhibiting extensive actin filaments (EFs; schematic in Figure 2C) and 10% of S9 follicles exhibiting larger, aberrant actin aggregate structures (AGs; schematic in Figure 2D) emanating from the ring canals and the surrounding cortical area (Figure 2E).

In contrast, the prevalence of both classes of early actin structures is dramatically increased in *pxt* mutants, with 10% exhibiting EF and 24% exhibiting AG in pxt^{f} follicles, and 17% exhibiting EF and 57% exhibiting AG in pxt^{EY} follicles (Figure 2, C–D′ and E, and Supplemental Figure S2A). To rule out any background-specific effects on early-actin-remodeling prevalence, we examined the incidence of early-actin-remodeling defects in the heteroallelic combination and found an intermediate phenotype, with 19% exhibiting EF and 45% exhibiting AG in $pxt^{EY03052/f01000}$ follicles ($pxt^{EY/f}$; Figure 2E and Supplemental Figure S2A). In addition, we used the GAL4/UAS system (Brand and Perrimon, 1993; Rorth, 1998) to perform rescue experiments to verify that loss of Pxt causes the early actin structures. Germline-specific overexpression of Pxt (UAS Pxt/*mat*αGAL4; $pxt^{EY/f}$) reduced the prevalence of early-actin-remodeling defects to 18% (6% EF; 12% AG) compared with controls (UAS Pxt/bal; $pxt^{EY/f}$ or *mat*αGAL4/bal; $pxt^{EY/f}$), which exhibited early-actin-remodeling defects in 43% (8% EF; 35% AG) and 70% (13% EF; 57% AG), respectively (Figure 2F and Supplemental Figure S2B). These data indicate that Pxt is required to prevent or restrict early actin remodeling during S9 of *Drosophila* follicle development.

Early actin remodeling does not affect oocyte polarity

Given the high prevalence of early actin structures in *pxt* mutants at S9, we wanted to determine whether such structures adversely affect other developmental events occurring during this time. During S9, oocyte polarity is being established, and slow cytoplasmic streaming from the nurse cells into the oocyte is occurring (Gutzeit, 1986; Theurkauf *et al.*, 1992). Therefore we wanted to determine whether oocyte polarity was disrupted by early actin remodeling in *pxt*-mutant follicles. We used immunofluorescence to assess whether the localization of two well-established oocyte polarity markers—Gurken and Staufen—are disrupted in *pxt*-mutant follicles. Gurken, a transforming growth factor α–like protein and epidermal growth factor receptor ligand, is required for dorsal specification and dorsal-ventral patterning of both the oocyte and embryo (Neuman-Silberberg and Schupbach, 1993). Gurken localizes to the dorsal-anterior corner of the oocyte in wild-type S9 follicles (Neuman-Silberberg and Schupbach, 1996; Figure 3, A–A′). In *pxt* mutants, Gurken localization is not altered, even in the presence of early actin structures (Figure 3, B–C′). Staufen, an mRNA-binding protein (St Johnston *et al.*, 1992), is a member of the posterior group genes (Schupbach and Wieschaus, 1986) and, as such, is required for posterior fate specification and anterior-posterior patterning in the oocyte and, subsequently, the embryo. In wild-type S9 follicles, Staufen localizes to and accumulates at the posterior of the oocyte (St Johnston *et al.*, 1991; Figure 3, D–D′). This posterior accumulation is unaltered in *pxt*-mutant follicles, including follicles exhibiting early actin structures (Figure 3, E–F′). These data indicate that neither loss of *pxt* nor early onset of actin remodeling substantially affects establishment of oocyte polarity, suggesting that slow cytoplasmic streaming is likely normal in *pxt* mutants.

Prevalence of early actin structures is reduced in later stages

We next wanted to consider what happens to the early actin structures as the follicle progresses through development. To address this, we quantified the prevalence of EF and AG in the subsequent stage of follicle development, S10A. We found that whereas the prevalence of early-actin-remodeling defects is unchanged for wild type, 10% (6% EF, 4% AG), it is significantly reduced in all *pxt*-mutant combinations, with 9% (5% EF, 4% AG) of pxt^{f}, 39% (6% EF, 33% AG) of pxt^{EY}, and 19% (5% EF, 14% AG) of $pxt^{EY/f}$ mutant follicles exhibiting defects (Figure 4, A and B, and Supplemental Figure S3A).

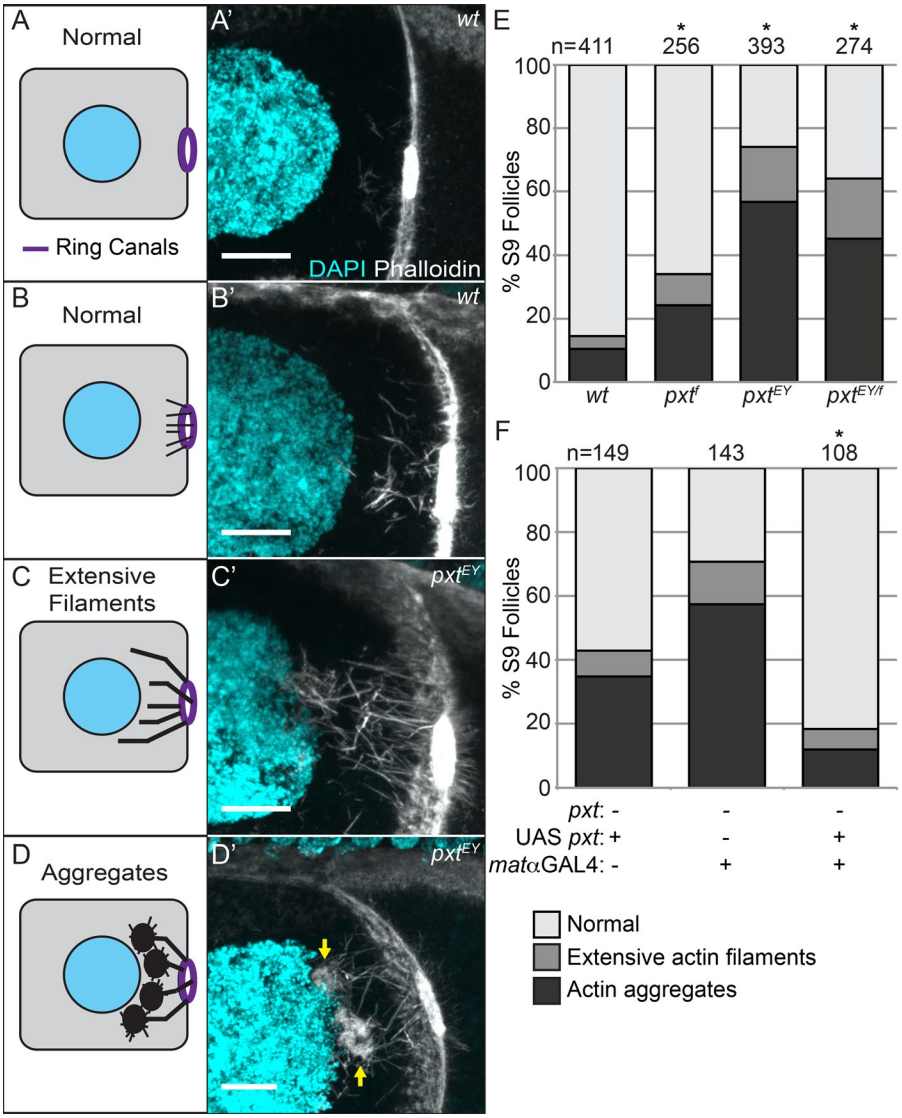

FIGURE 2: Early actin remodeling is highly penetrant in *pxt* mutants. (A–D) Schematics of a posterior nurse cell exhibiting normal or aberrant actin structures associated with the posterior ring canals during S9. (C′–D′) Maximum projections of confocal slices of posterior nurse cells of S9 follicles taken at 63× magnification. Anterior is to the left and posterior (i.e., the oocyte) is to the right. F-actin (phalloidin), white; DNA (DAPI), cyan. (A′, B′) Wild type, wt (*yw*). (C′, D′) pxt^{EY}. Images are representative and taken from multiple experiments. (E–F) Charts quantifying the percentage of S9 follicles exhibiting normal, extensive actin filament, and actin aggregate phenotypes for the indicated genotypes; the numbers of follicles scored are indicated above each bar (*n*). The posterior ring canals of wild-type follicles are either devoid of actin filaments (A–A′) or exhibit minimal actin filament structures extending toward the nurse cell nucleus (B–B′). In contrast, *pxt*-mutant S9 follicles exhibit much more extensive actin filaments (C–C′) and actin aggregate structures (D–D′, yellow arrows) emanating from the posterior ring canals. Quantification of these early actin structures reveals that they are highly penetrant in both *pxt* alleles and the heteroallelic combination. Whereas only 14% of wild-type S9 follicles exhibit early actin structures, this remodeling is dramatically increased in *pxt* mutants, with 34% of pxt^{f} S9, 74% of pxt^{EY}, and 64% of $pxt^{EY/f}$ follicles exhibiting early actin structures (E; $p < 0.001$ for pxt^{f}, pxt^{EY}, and $pxt^{EY/f}$ compared with wild type). Germline expression of *pxt* using the GAL4/UAS system rescues the early actin remodeling (F; $p < 0.001$ for UAS *pxt*/*mat*αGAL4; $pxt^{EY/f}$ compared with UAS *pxt*; $pxt^{EY/f}$ or *mat*αGAL4; $pxt^{EY/f}$). Scale bars, 10 μm. *$p < 0.001$ using global chi-squared tests.

Because early and aberrant actin structures are present in some S10A *pxt*-mutant follicles, we next wanted to determine whether they are also present at S10B and the relationship of such structures to canonical actin-remodeling events. During S10B, dynamic actin remodeling occurs within the nurse cells. Parallel actin filament bundles extend from the plasma membrane to form a cage around the nucleus, and the cortical actin is strengthened (Guild *et al.*, 1997; Huelsmann *et al.*, 2013). We previously showed that Pxt and, thus, PG signaling play critical roles in this remodeling. Indeed, *pxt* mutants exhibit decreased bundle formation and loss of cortical actin integrity (Figure 1, F–G′ compared with E–E′; Tootle and Spradling, 2008; Groen *et al.*, 2012). Thus the early actin structures could contribute to the observed S10B actin-remodeling defects in *pxt* mutants. If these aberrant structures preclude canonical actin remodeling at S10B, then AGs should not be observed in the presence of bundle formation. We quantified the prevalence of AGs in the presence or absence of canonical actin remodeling in S10B follicles. We found that, during S10B, the majority of follicles exhibiting aggregates also had bundle formation. Indeed, 4% (4% AG with bundles, 0% AG without bundles) of wild-type follicles, 10% (8% AG with bundles, 2% AG without bundles) of pxt^{f}, 21% (14% AG with bundles, 7% AG without bundles) of pxt^{EY}, and 31% (24% AG with bundles, 7% AG without bundles) of $pxt^{EY/f}$ exhibit actin aggregates (Figure 4C and Supplemental Figure S3B). These data indicate that early and aberrant actin remodeling observed in *pxt* mutants does not preclude canonical remodeling at S10B. In addition, they reveal that the aberrant early actin structures observed in *pxt*-mutant follicles decrease in incidence with developmental time.

Follicle death is increased in *pxt* mutants

One mechanism that could account for the decreased frequency of the early actin structures during development is increased follicle death. Under optimal conditions, follicle death is infrequent and restricted to well-defined, developmental checkpoints. The first checkpoint, which is linked to the nutritional status of the fly, occurs in region 2 of the germarium (Drummond-Barbosa and Spradling, 2001). The second checkpoint occurs at S8 and is governed by hormone signaling, nutrition, environmental factors, and follicle cell quality (Giorgi and Deri, 1976; Buszczak *et al.*, 1999; Chao and Nagoshi, 1999; Carney and Bender, 2000; Nezis *et al.*, 2000). In addition, S14 follicles can undergo resorption if not laid (reviewed in Spradling, 1993). Cursory examination of *pxt*-mutant ovarioles suggested that follicle death might be occurring abnormally (at S9 or later), leading us to hypothesize that aberrant follicle death may explain the apparent decrease in early actin structures with developmental time. To

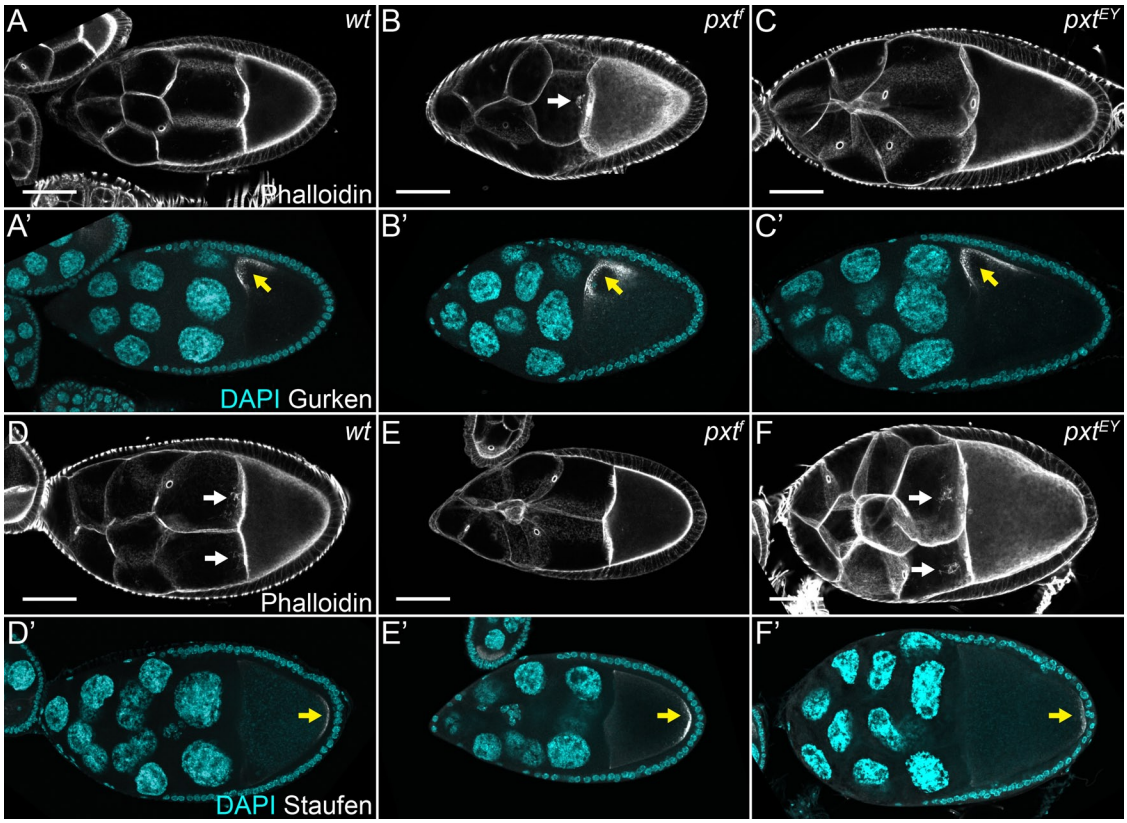

FIGURE 3: Oocyte polarity is normal in *pxt* mutants. (A–F′) Maximum projections of confocal slices of S9 follicles taken at 20× magnification; anterior is to the left. (A–F) F-actin (phalloidin), white. (A′–C′) Merged images: DNA (DAPI), cyan; Gurken, white. (D′–F′) Merged images: DNA (DAPI), cyan; Staufen, white. (A–A′, D–D′) Wild type, wt (*yw*). (B–B′, E–E′) pxt^{f}. (C–C′, F–F′) pxt^{EY}. In wild-type S9 follicles (A), Gurken localizes to the dorsal-anterior corner of the oocyte (A′, yellow arrow). In pxt^{f} (B) and pxt^{EY} (C) mutants, the localization of Gurken is not disrupted (B′–C′, yellow arrows), even when actin aggregates are present (B, white arrow). In wild-type S9 follicles (D), Staufen localizes to the posterior of the oocyte (D′, yellow arrow), including in follicles with early actin structures (D, white arrows). In pxt^{f} (E) and pxt^{EY} (F) mutants, Staufen localization to the posterior of the oocyte is unchanged (E′–F′, yellow arrows), even when actin aggregates are present (F, white arrows). Scale bars, 50 μm.

test this hypothesis, we quantified both normal follicle death (the percentage of ovarioles exhibiting follicle death at the S8 checkpoint) and aberrant follicle death (the percentage of ovarioles exhibiting follicle death occurring at S9 or later). Follicle death is easily assessed using DNA morphology by scoring for DNA condensation and/or fragmentation using 4′,6-diamidino-2-phenylindole (DAPI) staining. In wild type, the vast majority of ovarioles examined showed no follicle death (Figure 5, A and B, and Supplemental Figure S4), whereas 9% showed signs of follicle death at S8 (Figure 5, A and C), and only 2% of ovarioles examined showed aberrant follicle death (Figure 5A). In *pxt* mutants, follicle death at the S8 checkpoint (Figure 5, D and F) was elevated to the same levels in both mutant backgrounds (16% for pxt^{f} and pxt^{EY}, $p < 0.0001$ for each genotype compared with wild type; Figure 5A and Supplemental Figure S4). However, although aberrant follicle death was only slightly elevated in pxt^{EY} ovarioles (6%, $p < 0.0001$), it was dramatically elevated in pxt^{f} ovarioles (38%, $p < 0.0001$; Figure 5, A and E–G, and Supplemental Figure S4) compared with wild type. These data suggest that increased follicle death may account for some, but not all, of the decrease in the prevalence of early actin structures over developmental time.

Because increased follicle death is unlikely to fully account for the decreased incidence of early actin structures throughout development, we speculate that these structures may undergo active remodeling. Unfortunately, the extent to which this remodeling occurs cannot be assessed at this time due to technical limitations. In our hands, germline expression of a variety of actin-labeling tools for use in live imaging result in numerous cytoskeletal defects, including early actin remodeling (Spracklen, Fagan, Lovander, and Tootle, unpublished data). Thus it is not possible to use live imaging to determine whether such remodeling is occurring.

Hts-RC and Villin localize to early actin structures

We hypothesized that the early actin remodeling observed in *pxt*-mutant follicles is due to the misregulation of specific actin-binding proteins that temporally regulate actin remodeling downstream of PG signaling. To identify such proteins, we used an immunofluorescence-based approach to identify factors involved in the formation and/or maintenance of early actin structures. We hypothesized that we would observe two categories of actin-binding proteins that localize to early actin structures. The first category was expected to comprise factors that localize to all early actin structures. Such proteins may contribute to the formation and/or maintenance of these structures or may simply bind to them. The second category was expected to be made up of factors that localize specifically to the aberrant early actin structures in *pxt*-mutant but not wild-type S9 follicles. Such factors may be driving the formation of these

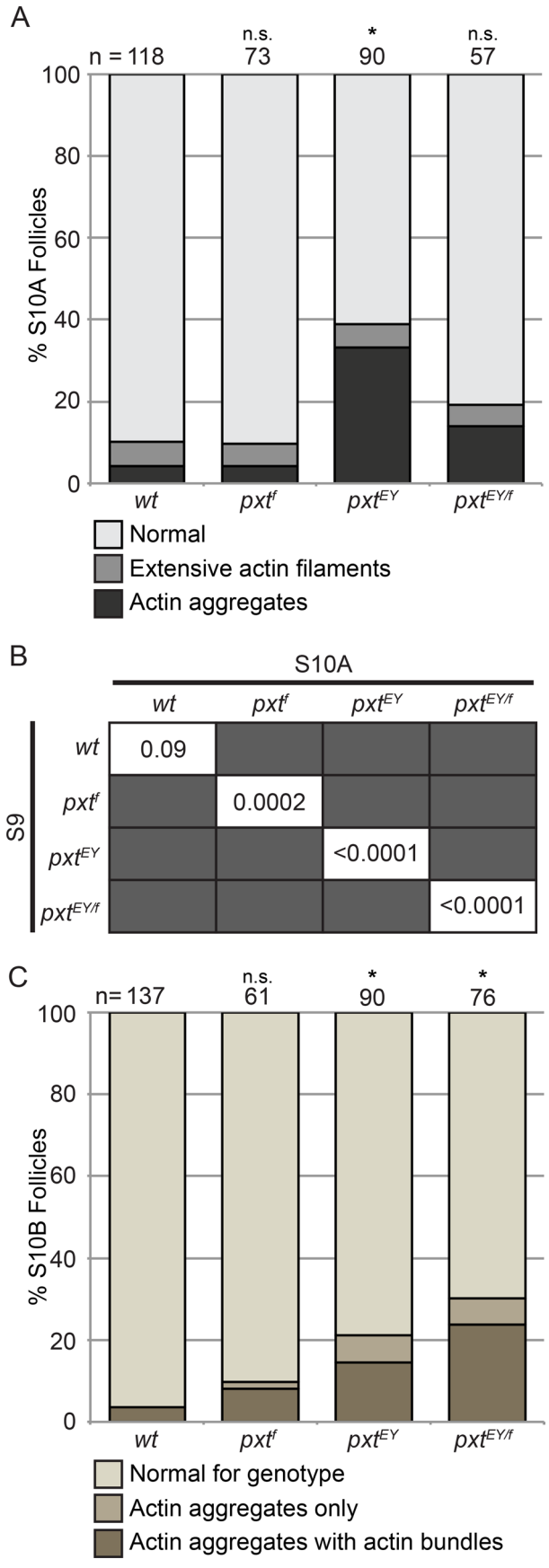

FIGURE 4: The prevalence of aberrant, early actin structures in *pxt* mutants decreases in later stages of development. (A) Chart quantifying the percentage of S10A follicles exhibiting normal, extensive actin filament, and actin aggregate phenotypes for the indicated genotypes; the numbers of follicles scored are indicated above each bar (*n*). (B) Table of *p* values from global chi-squared tests comparing the prevalence of the early actin structures at S9 and S10A for a given genotype. (C) Chart quantifying the percentage of S10B exhibiting normal actin remodeling for the indicated genotype (see *Materials and Methods* for more details), only actin aggregates, and actin aggregates with bundle formation. The prevalences of the early actin structures in pxt^{f} and $pxt^{EY/f}$ at S10A are not statistically different from those for wild-type follicles, whereas the level of early structures for pxt^{EY} at S10A is significantly higher than that in wild-type follicles (A). Of note, the prevalence of these structures in all *pxt* mutants is reduced in S10A compared with S9 (B). During S10B, wild-type follicles undergo dynamic actin remodeling, including the generation of parallel actin bundles; this remodeling is aberrant in *pxt* mutants. Actin aggregates alone or with bundles are observed at a significantly higher level in pxt^{EY} and $pxt^{EY/f}$ than in wild-type S10B follicles (C). $^{*}p < 0.05$ using global chi-squared tests.

structures and are likely to be regulated by PG signaling. We identified two actin-binding proteins that fall into the former category and one that falls into the latter category.

Hts, the *Drosophila* homologue of Adducin, was previously shown to play critical roles during early cyst formation, oocyte specification, and ring canal formation and maintenance (Yue and Spradling, 1992). Previously Hts-RC (Robinson *et al*., 1994; Petrella *et al*., 2007) was reported to form filamentous structures associated with actin filaments in dying wild-type S8 follicles (Chao and Nagoshi, 1999). On the basis of the similarity between the actin structures that were described in that report and the early actin structures that we observe in *pxt* mutants, we asked whether Hts-RC localizes to the early actin structures in wild-type and/or *pxt*-mutant follicles. We found that Hts-RC strongly localizes to EF structures in both wild-type (Figure 6, A–A″, arrowheads) and *pxt*-mutant (Figure 6, B–C″, arrowheads) follicles, where it forms filament structures that are highly similar to their actin counterparts. Of interest, Hts-RC appears to be excluded from AG structures in both wild-type (unpublished data) and *pxt*-mutant follicles (Figure 6, B–C″, asterisks). This reveals that Hts-RC is associated with filamentous early actin structures, but that this localization is unlikely to be regulated downstream of PG signaling.

Villin (*Drosophila* Quail) is an actin-bundling protein that was shown to be required for parallel actin bundle formation at S10B (Mahajan-Miklos and Cooley, 1994b). Because the extensive early actin filaments that we observe in wild-type and *pxt*-mutant S9 follicles appear structurally similar to the canonical parallel actin filament bundles observed during S10B, we next asked whether Villin localizes to the early actin structures. Consistent with previous reports (Mahajan-Miklos and Cooley, 1994b), we find that Villin is uniformly distributed throughout the nurse cell cytoplasm and localizes to both the cortical regions and ring canals of wild-type S9 follicles. In wild-type follicles possessing early actin structures, Villin also decorates early actin filaments as distinct puncta distributed along their length (Figure 6, D–D″). Homozygosity for either allele of *pxt* does not alter Villin distribution throughout the cytoplasm or localization to the nurse cell cortical regions or ring canals. In addition, Villin localization to early actin structures is similar to that of wild type in *pxt*-mutant S9 follicles (Figure 6, E–F″). These data reveal that Villin is associated with early actin structures but is unlikely to be regulated downstream of PG signaling. Similarly, we previously showed that Villin is not a target of PG signaling during canonical actin remodeling during S10B (Groen *et al*., 2012).

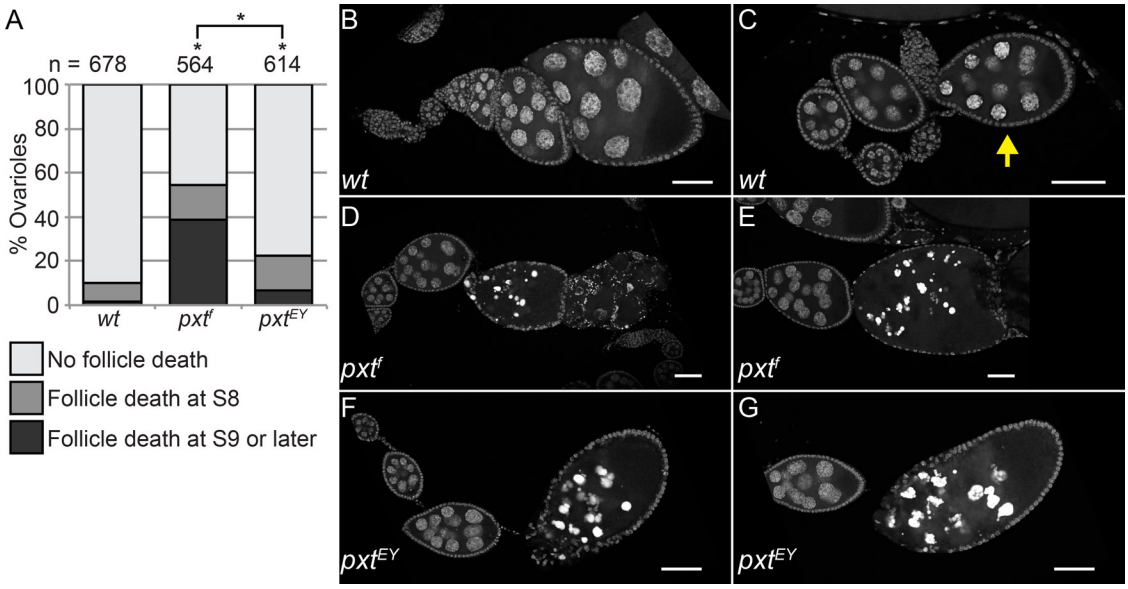

FIGURE 5: Follicle death is increased in *pxt* mutants. (A) Chart quantifying the percentage of wild-type and *pxt* mutant ovarioles containing a dying follicle either at the S8 checkpoint or at S9 or later in development; the numbers of ovarioles scored are indicated above each bar (*n*). Follicle death was assessed by DNA condensation and fragmentation. (B–G) Maximum projections of confocal slices of S9 follicles taken at 20× magnification; DNA (DAPI), white. (B, C) Wild type, wt (*yw*). (D, E) pxt^{f}. (F, G) pxt^{EY}. The vast majority (89%) of wild-type ovarioles showed no signs of follicle death (A), as evident by DNA morphology (B), whereas 9% exhibited follicle death at the S8 checkpoint, as evident by DNA condensation (C, yellow arrow) or fragmentation (not shown). Infrequently (2%), wild-type ovarioles exhibit abnormal follicle death (follicle death occurring ≥S9) (A). In contrast, pxt^{f} ovarioles show a mild increase in follicle death at S8 (16%; A, D) and a dramatic increase in abnormal follicle death (38%; A, E; $p < 0.001$ for pxt^{f} compared with wild type), whereas pxt^{EY} ovarioles show a mild increase in follicle death at the S8 checkpoint (16%; A, F) and abnormal death (6%; A, G) compared with wild type ($p < 0.001$ pxt^{EY} compared with wild type). Of note, the level of follicle death in pxt^{f}-mutant ovarioles is significantly higher than that in pxt^{EY} ($p < 0.001$). Scale bars, 50 μm. *$p < 0.001$ using global chi-squared tests.

Ena localization to early actin structures at S9 is enhanced in *pxt* mutants

In addition to Hts and Villin, we also examined the localization of Ena, the sole Ena/VASP family member found in *Drosophila* (Gertler *et al.*, 1996). Ena is an actin elongation and anticapping factor (reviewed in Bear and Gertler, 2009). Previous studies showed that Ena regulates the actin cytoskeleton during oogenesis. Specifically, Ena mediates border cell migration (Gates *et al.*, 2009; Lucas *et al.*, 2013) and plays a critical role in the formation of the parallel actin filament bundles produced during S10B (Gates *et al.*, 2009). Owing to Ena's established role in promoting actin remodeling during oogenesis, we hypothesized that misregulation of Ena could drive early actin remodeling. Indeed, we found that Ena preferentially localizes to early actin structures in *pxt*-mutant S9 follicles. In wild-type follicles possessing early actin structures, Ena occasionally localizes to the actin filaments and actin aggregates as distinct puncta (Figure 7, B–B″ compared with A–A″, and Supplemental Movie S1, B compared with A). This localization is more robust and more frequent in *pxt*-mutant follicles (Figure 7, C–D″, and Supplemental Movie S1, C and D). The punctate nature of Ena localization is expected, as Ena exhibits a punctate appearance at the barbed ends of the growing actin filaments at S10B (see later discussion of Figure 9; Gates *et al.*, 2009). Because Ena is highly expressed in the nurse cell cytoplasm, it was not feasible to simply score Ena localization by eye. To circumvent this, we blindly scored 63× confocal images to quantify the preferential Ena localization. As we expected, this revealed that few wild-type follicles exhibited Ena localization to the early actin structures (2/12), whereas the majority of *pxt*-mutant follicles (5/11 pxt^{f}, 7/10 pxt^{EY}, and 4/6 $pxt^{EY/f}$) exhibited Ena localization. These data suggest that PG signaling may negatively regulate Ena to prevent early actin remodeling at S9. Alternatively, it remains possible that the observed increase in Ena localization is simply a consequence of the high frequency of these structures in the *pxt* mutants.

Ena genetically interacts with *pxt*

To distinguish between these possibilities, we performed genetic interaction studies. If misregulation of Ena results in early actin remodeling in the absence of PG signaling, then we expected that genetic reduction of *ena* would suppress early actin remodeling in a *pxt*-mutant background. To test this, we generated animals that were heterozygous for null alleles ($ena^{GC1/+}$ or $ena^{GC5/+}$) or for an allele carrying a point mutation in the EVH1 domain ($ena^{210/+}$) of Ena in a homozygous *pxt*-mutant background ($pxt^{EY/f}$) and assessed the prevalence of early actin structures at S9. We found that heterozygosity for loss of *ena* strongly suppressed aberrant actin remodeling in *pxt* mutants (Figure 8A and Supplemental Figure S5). The *pxt*-mutant ($pxt^{EY/f}$) S9 follicles exhibited 59% prevalence of early actin structures (20% EF, 39% AG), whereas S9 follicles combining heterozygous loss of *ena* with homozygous loss of *pxt* exhibited significantly decreased incidence of early-actin-remodeling defects: $ena^{210/+}$; $pxt^{EY/f}$, 7% (2% EF, 5% AG); $ena^{GC1/+}$; $pxt^{EY/f}$, 14% (3% EF, 11% AG); and $ena^{GC5/+}$; $pxt^{EY/f}$, 4% (1% EF, 3% AG). These effects are likely due to a specific role of Ena in the *pxt*-mutant background, as *ena* heterozygotes do

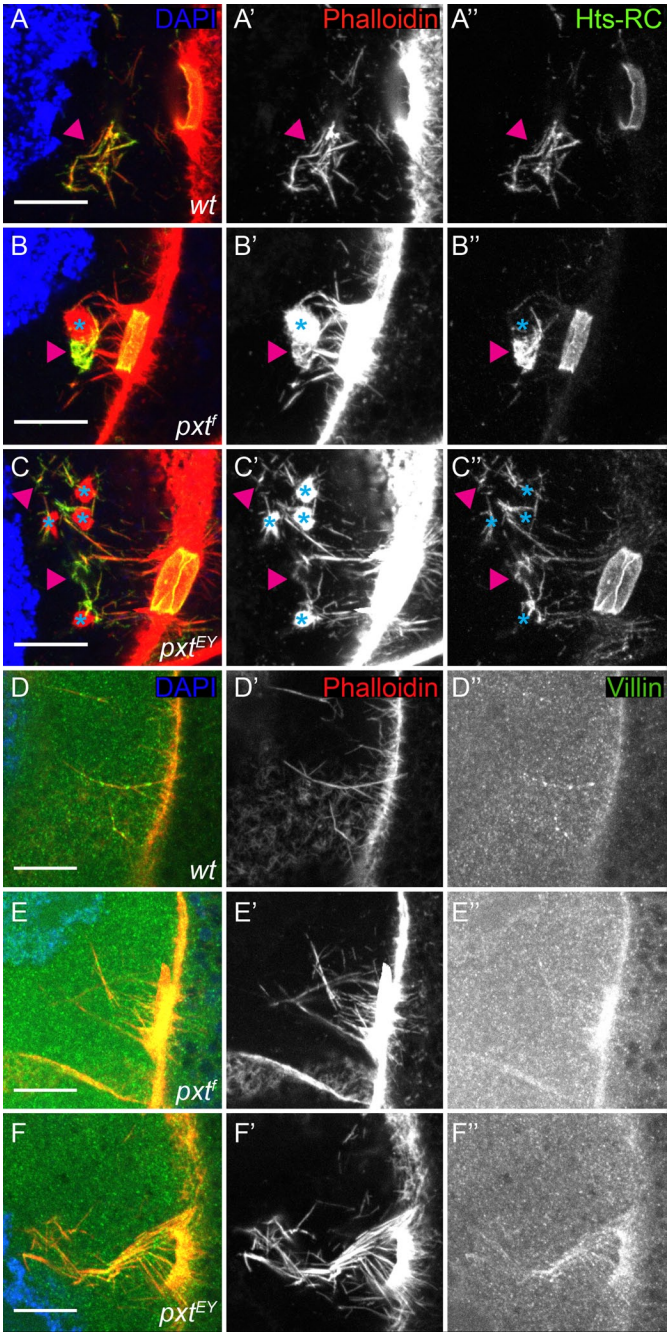

FIGURE 6: Hts-RC and Villin both localize to early actin structures in wild-type and *pxt* mutant S9 follicles. (A–F″) Maximum projections of confocal slices of the posterior nurse cells of S9 follicles taken at 63× magnification. Anterior is to the left and posterior (i.e., the oocyte) to the right. (A–C) Merged images: DNA (DAPI), blue; F-actin (phalloidin), red; Hts-RC, green. (A′–C′) F-actin (phalloidin), white. (A″–C″) Hts-RC, white. (D–F) Merged images: DNA (DAPI), blue; F-actin (phalloidin), red; Villin, green. (D′–F′) F-actin (phalloidin), white. (D″–F″) Villin, white. (A–A″, D–D″) Wild type, wt (*yw*). (B–B″, E–E″) pxt^{f}. (C–C″, F–F″) pxt^{EY}. Hts-RC localizes to early actin structures in both wild-type (A–A″) and *pxt*-mutant (B–C″) S9 follicles, where it colocalizes with actin filament structures (magenta arrowheads, A–C″), but not actin aggregates (cyan asterisks, B–C″). Villin localizes as discrete puncta along the early actin filaments in both wild-type (D–D″) and *pxt*-mutant (E–F″) S9 follicles. Scale bars, 10 μm.

not display reduced prevalence of early actin structures compared with wild-type follicles (Supplemental Figure S6). These data indicate that Ena is required for early actin remodeling in *pxt* mutants.

The strength of the suppression of the *pxt*-mutant phenotype by loss of one copy of *ena*, in combination with our observation that the cytoplasmic level of Ena in the *pxt*-mutant nurse cells appeared to be higher than that of wild-type S9 follicles (Figure 7), led us to examine whether Pxt affects the expression of Ena. We found that in both whole-ovary and S9-specific lysates both mRNA and protein levels are not significantly altered in *pxt* mutants (Figure 8, B–E). This suggests that PG signaling, either directly or indirectly, regulates Ena localization and/or activity by another mechanism, such as through posttranslational modifications or altered protein–protein interactions. Together these data are consistent with a model in which, at S9, Pxt leads to the production of a PG or PGs that elicit a signaling cascade, which ultimately, and by as-yet-unknown mechanisms (direct or indirect), controls Ena localization and/or activity to prevent inappropriate actin remodeling, thus restricting actin remodeling to the correct development time.

Ena localization is disrupted at S10B

Previously we showed that *pxt*-mutant follicles display a substantially reduced ability to form parallel actin filament bundles at S10B and thus fail to undergo nurse cell dumping (Tootle and Spradling, 2008; Groen *et al.*, 2012; Figure 1, F–G′ compared with E–E′). Previous studies indicated that Ena is required for actin filament bundle elongation and localizes to their barbed, or growing, ends (Gates *et al.*, 2009), which are positioned proximal to the nurse cell membranes (Guild *et al.*, 1997). Using immunofluorescence and confocal microscopy, we find that Ena localization to both the barbed ends of actin filament bundles (puncta; examples circled in Figure 9) and nurse cell membranes is reduced in *pxt* mutants compared with wild type at S10B (Figure 9, B–C‴ compared with A–A‴). Similar to what we found during S9, loss of PG signaling does not affect Ena expression at either the mRNA (Tootle *et al.*, 2011) or protein level (Supplemental Figure S7). Of note, the extent of the reduction in Ena localization corresponds to the severity of the S10B phenotype in *pxt* mutants, such that when there are practically no bundles, there is similarly little to no Ena (Figure 9, C–C‴). Because Ena is believed to be required for bundle formation/elongation (Gates *et al.*, 2009), this leads us to hypothesize that the reduction in Ena localization to the sites of bundle formation is one of the causes of the bundle defects observed in *pxt* mutants. Together these data (Figures 7–9) suggest that PG signaling may be required to regulate Ena localization/activity throughout mid- to late-stage oogenesis, leading us to propose a model in which PG signaling temporally regulates the onset of actin remodeling during *Drosophila* oogenesis, at least in part, by restricting Ena localization/activity earlier in oogenesis (S9) and promoting appropriate Ena localization/activity later in oogenesis (S10B). Whether this regulation is achieved through a direct or an indirect mechanism remains unclear.

DISCUSSION

PGs have a wide variety of physiological functions in vertebrates. However, the extent to which their functions are conserved in insects is less clear. Although PGs regulate immunity and secretions from malpighian tubules, the rectum, and salivary glands, their best-characterized roles in insects are during oocyte development and female reproduction (reviewed in Stanley and Kim, 2011). *Drosophila* Pxt is a COX1-like enzyme and is required for female fertility due to multiple roles during oogenesis (Tootle and Spradling, 2008;

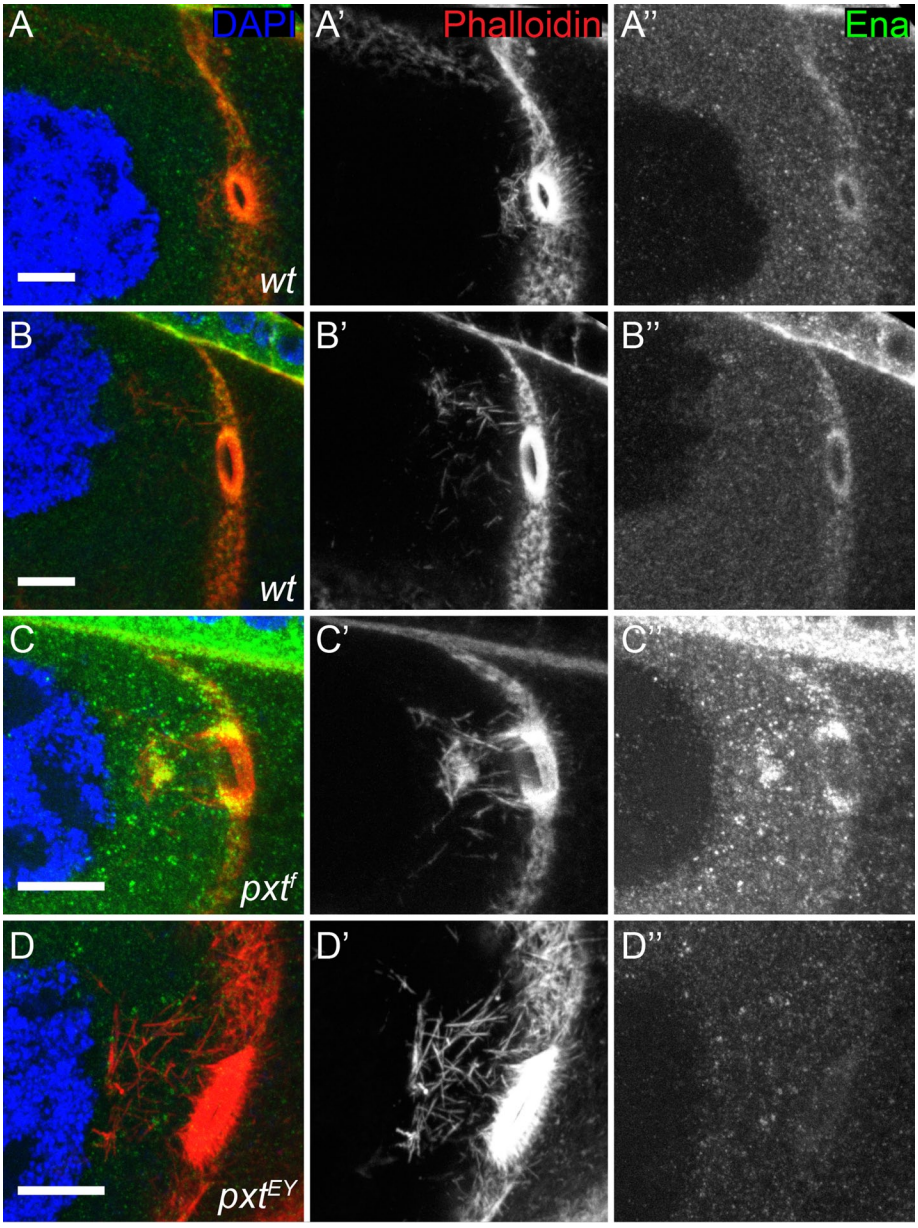

FIGURE 7: Ena preferentially localizes to early actin structures in *pxt*-mutant follicles. (A–D″) Maximum projections of confocal slices of S9 follicles taken at 63× magnification. Anterior is to the left and posterior (i.e., the oocyte) to the right. (A–D) Merged images: DNA (DAPI), blue; F-actin (phalloidin), red; Ena, green. (A′–D′) F-actin (phalloidin), white. (A″–D″) Ena, white. (A–B″) Wild type, wt (*yw*). (C–C″) pxt^{f}. (D–D″) pxt^{EY}. Although the majority of wild-type S9 follicles fail to exhibit Ena puncta localizing to the early actin structures (A–A″; 10/12 images blindly scored), weak Ena localization occasionally is observed (B–B″; 2/12 images). Conversely, Ena generally localizes to both the extensive filaments as puncta (D–D″) and aggregates (C–C″) observed in *pxt* mutants (5/11 pxt^{f}, 7/10 pxt^{EY}, and 4/6 $pxt^{EY/f}$ images). Images are representative and taken from multiple experiments. Scale bars, 10 μm.

Tootle *et al.*, 2011). PGs likely have additional functions in *Drosophila*, as *pxt*-mutant adults eclose later and at reduced numbers, exhibit a low frequency of cuticle-patterning defects, appear to have a reduced lifespan and are sickly, and exhibit abnormal-looking adult organs (i.e., gut and malpighian tubules). Thus *Drosophila* can likely be used to define the evolutionarily conserved roles of PGs in multiple tissues.

Here we provide strong evidence that PGs temporally regulate cytoplasmic F-actin formation and elongation in *Drosophila* nurse cells. Genetic loss of Pxt results in a highly penetrant, early induction of filamentous and aggregated actin structures in the posterior nurse cells of S9 follicles. Of importance, overexpression of Pxt suppresses early actin remodeling, and similar structures are observed at a low frequency in wild-type follicles. Previously we showed that Pxt is also required for cortical actin integrity and bundle formation during S10B (Tootle and Spradling, 2008; Groen *et al.*, 2012). Together these data lead to a model in which, during S9, Pxt-dependent PG production initiates a signaling cascade that prevents or restricts early actin remodeling, whereas during S10B, Pxt-dependent PG signaling induces actin-remodeling events necessary for nurse cell dumping. These opposing activities could be achieved through different PGs at S9 and S10B, or the same PG may be produced at both stages but elicit distinct signaling cascades. We favor the first possibility, as exogenous PGE_2 inhibits, whereas $PGF_{2\alpha}$ promotes in vitro nurse cell dumping and $PGF_{2\alpha}$ restores dumping in the presence of COX inhibitor treatment or genetic loss of Pxt (Tootle and Spradling, 2008; Groen *et al.*, 2012). Thus we hypothesize that Pxt leads to PGE_2 signaling at S9 and $PGF_{2\alpha}$ signaling at S10B.

Although early actin remodeling in the posterior nurse cells is observed in response to certain stresses and in a few mutant backgrounds, our understanding of how these structures form and the consequences of such formation is severely limited. Overexpression of death-inducing factors in the follicle cells or starvation results in follicle death at S8/9 and the accumulation of actin filaments and aggregates (Chao and Nagoshi, 1999). Of interest, these actin structures colocalize with Hts-RC, similar to what we observed in both wild type and *pxt* mutants. In addition, expression of active Dcp-1 disrupts the actin cytoskeleton within the nurse cells at S10B, suggesting that limiting caspase activation may prevent the destruction of the nurse cell cytoskeleton (Peterson *et al.*, 2003). Furthermore, loss of Midway, a diacylglycerol acyltransferase, causes S8 checkpoint death, and the dying follicles accumulate extensive actin filaments in the posterior nurse cells (Buszczak *et al.*, 2002). Thus early actin structures may either cause or be caused by the induction of follicle death.

If premature actin remodeling in *pxt* mutants is either driving or caused by induction of follicle death, then the prevalence of the actin structures should be similar to the levels of death. This is not what we observe, as 34% of pxt^{f} and 74% of pxt^{EY} S9 follicles exhibit early actin structures, whereas there is a much higher level of follicle death in pxt^{f} (54% death), the allele with a lower frequency of early actin structures, than in the pxt^{EY} allele (22% death). These data suggest that early actin structures can form and not result in follicle

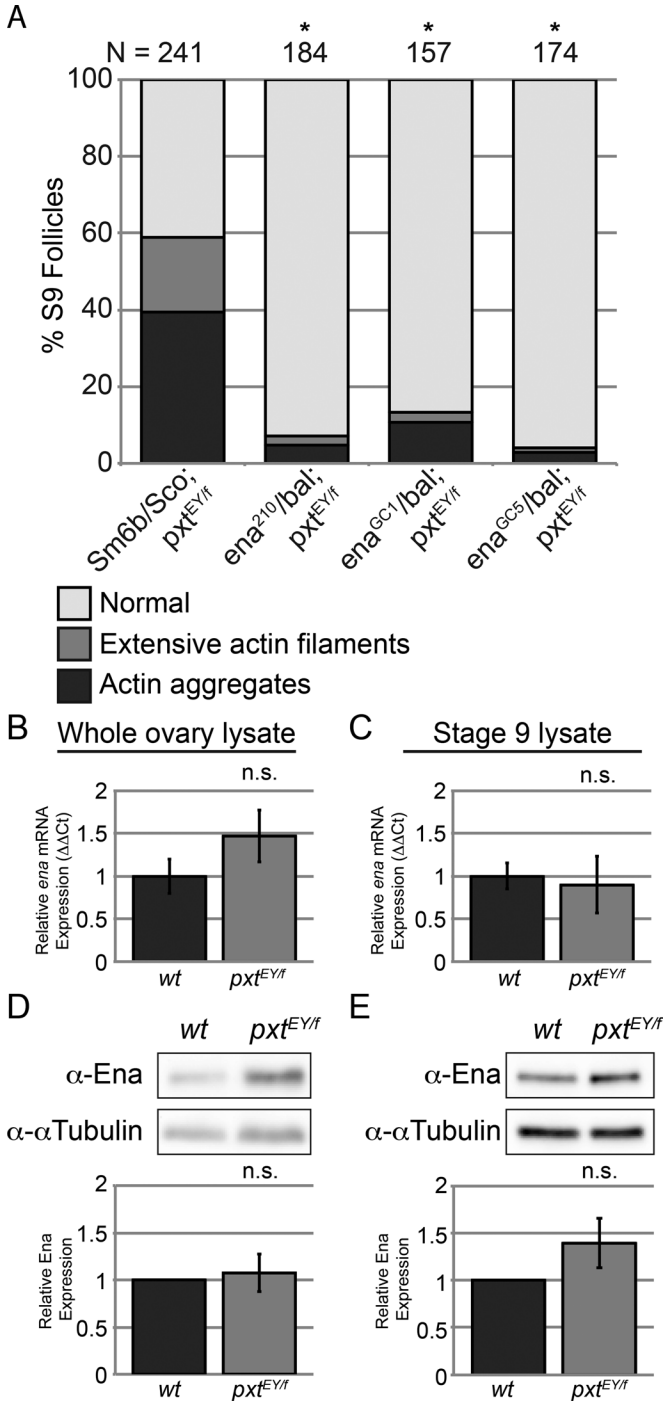

FIGURE 8: A reduction in Ena suppresses early actin remodeling in *pxt* mutants. (A) Chart quantifying the percentage of S9 follicles exhibiting normal, extensive actin filament, and actin aggregate phenotypes for the indicated genotypes; the numbers of follicles scored are indicated above each bar (*n*). (B, C) Charts quantifying the normalized levels of *ena* mRNA for whole ovary and S9, respectively. (D, E) Representative Western blots for Ena levels and charts quantifying the normalized levels of Ena in whole ovaries and S9, respectively, for the indicated genotypes. Loss of Pxt ($pxt^{EY/f}$) results in early actin remodeling; heterozygosity for mutations in *ena* (ena^{210}, ena^{GC1}, and ena^{GC5}) block this early actin remodeling (A). Ena mRNA (B, C) and protein (D, E) levels are unchanged in *pxt*-mutant ovaries and S9 follicles. In A, $*p < 0.001$ using global chi-squared tests. In B–E, n.s. = $p > 0.05$ using a two-sample *t* test, unequal variance.

death and that follicles can die without forming such structures. Thus the function of these early actin structures remains unclear.

These early actin structures may function to assess whether the nurse cells are capable of the dramatic S10B remodeling events. In this case, small structures form and are rapidly depolymerized, as few wild-type S9 follicles exhibit visible, early actin structures. Supporting this idea, we find that strong germline expression of actin-labeling tools, which likely stabilize actin structures, result in increased frequency and size of these structures (Spracklen, Fagan, Lovander, and Tootle, unpublished observations). Alternatively, the early actin structures may regulate nuclear position. Indeed, Hts-RC—one of the factors we find associated with the early actin structures—localizes to a perinuclear actin meshwork that maintains nuclear position during nurse cell dumping (Huelsmann *et al.*, 2013). Defining the function of these early actin structures will require further analyses of their structure, dynamics, and regulation.

Our data are consistent with a model in which both the early actin remodeling during S9 and the inhibition of canonical actin remodeling during S10B observed in *pxt* mutants are due, at least in part, to misregulation of Ena, the sole *Drosophila* Ena/VASP family member (Gertler *et al.*, 1996). Supporting this model, we find that whereas the actin regulators Hts-RC and Villin localize the early actin structures in both wild-type and *pxt* mutant follicles, Ena preferentially localizes to the early actin structures in *pxt* mutants. Furthermore, a reduction in Ena level suppresses the early actin remodeling observed in *pxt*-mutant S9 follicles but has no effect on the prevalence of those structures in a wild-type background. Ena was shown to promote actin remodeling during S10B (Gates *et al.*, 2009). Of interest, Ena localization to the sites of canonical F-actin elongation is reduced in *pxt* mutants during S10B. The alterations in Ena localization in *pxt* mutants during both S9 and S10B are not due to changes in mRNA (Tootle *et al.*, 2011) or protein expression. These data led us to hypothesize that Pxt-dependent production of PGs results in the activation of signaling cascades that either directly or indirectly lead to altered Ena localization/activity. Ena may be regulated by protein–protein interactions, its antagonist capping protein, or phosphorylation (reviewed in Reinhard *et al.*, 2001). Of interest, loss of kinases known to regulate Ena/VASP proteins—PKA (Butt *et al.*, 1994; Gertler *et al.*, 1996; Lambrechts *et al.*, 2000) and Abelson tyrosine kinase (Gertler *et al.*, 1995, 1996; Comer *et al.*, 1998; Tani *et al.*, 2003; Maruoka *et al.*, 2012)—also results in early actin remodeling (Lane and Kalderon, 1995; Baum *et al.*, 2000; Gates *et al.*, 2009).

Although PG signaling is known to regulate VASP (Halbrugge *et al.*, 1990; Nolte *et al.*, 1991; Butt *et al.*, 1994; Horstrup *et al.*, 1994; Blume *et al.*, 2007), the extent to which the other homologues—Mena and Ena/VASP-like (Evl)—are regulated by PG signaling is unclear. Given that Ena exhibits a higher level of homology to Mena and Evl than to VASP (Gertler *et al.*, 1996), PG signaling is likely to regulate all three mammalian forms. Uncovering the means by which PG signaling regulates, either directly or indirectly, *Drosophila* Ena to temporally regulate actin remodeling during oogenesis is expected to reveal conserved mechanisms through which PG signaling modulates the activity of this family of actin regulators. Such mechanisms are likely to play critical roles not only during development, but also in human diseases, including heart disease and cancer (Pula and Krause, 2008; Yuhki *et al.*, 2011; Allaj *et al.*, 2013).

MATERIALS AND METHODS

Fly strains

Fly stocks were maintained at 21°C on standard cornmeal–agar–yeast food. Flies were fed with wet yeast paste daily and aged for

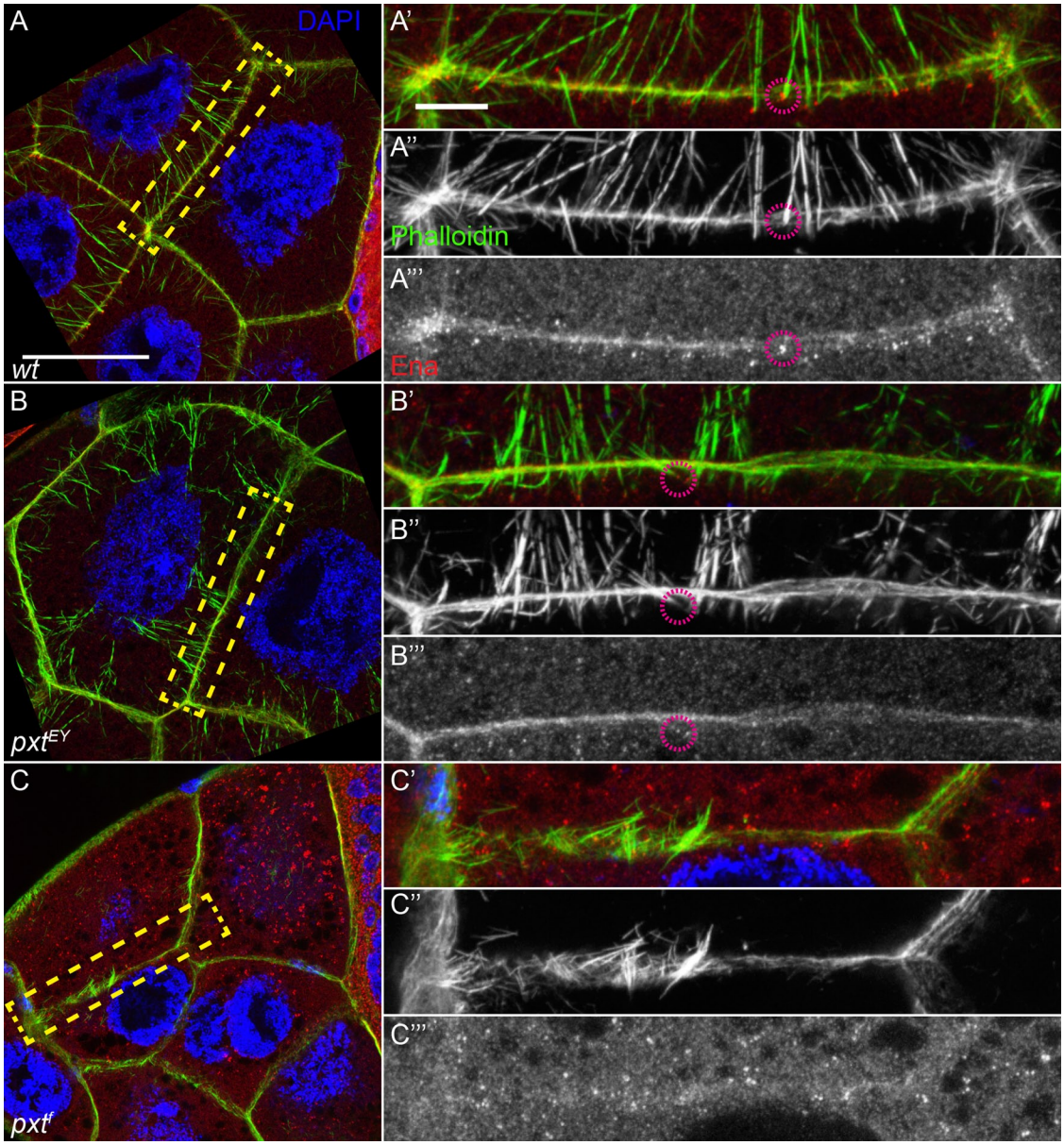

FIGURE 9: Ena localization to the barbed ends of actin filament bundles is disrupted in *pxt* mutants during S10B. (A–C) Maximum projections of confocal slices of S10B follicles taken at 63×magnification. Anterior is to the left and posterior (i.e., the oocyte) to the right. (A′–C‴) Magnified insets of region indicated by yellow box in A–C. (A–C′) Merged images: DNA (DAPI); F-actin (phalloidin), green; Ena, red. (A″–C″) F-actin (phalloidin), white. (A‴–C‴) Ena, white. (A′–A‴) Wild type, wt (*yw*). (B–B‴) pxt^{EY}. (C–C‴) pxt^{f}. In wild-type follicles, Ena localizes to the barbed, or growing, ends of actin filament bundles as distinct puncta (A; dashed magenta circles, A′–A‴) and to the nurse cell membranes. This localization is diminished in *pxt* mutants (B; magenta circles, B′–B‴; and C′–C‴ compared with A′–A‴). The extent of this reduction is dependent on the severity of actin-remodeling defects in *pxt* mutants (C–C‴ compared with B–B‴). Scale bars, 50 μm (A–C) or 10 μm (A′–C‴).

3–5 d for ovary analyses, including quantification of early actin remodeling defects, immunofluorescence, immunoblotting, and quantitative real-time PCR. *yw* was used as the wild-type control in experiments, except where indicated. $pxt^{EY03052}$ (referred to as pxt^{EY} in all of the figures), ena^{210}, ena^{GC1}, ena^{GC5}, and maternal α-tubulin Gal4 (matα; second chromosome) fly stocks were obtained from the Bloomington *Drosophila* Stock Center (Bloomington, IN); pxt^{f01000} (referred to as pxt^{f} in all of the figures) was obtained from Harvard Exelixis (Cambridge, MA); and UASp *pxt* was generated as previously described (Tootle and Spradling, 2008).

Immunofluorescence

Whole-mount samples were fixed using a protocol designed to better preserve actin structures (modified from Frydman and Spradling, 2001). In short, whole ovaries were dissected out in room-temperature Grace's insect media (Lonza, Walkersville, MD), and the ovarioles were teased apart using sharpened needles to remove the muscle sheath. Samples were then fixed for 10 min at room temperature in 4% paraformaldehyde, 2% Triton X-100, and 1 U/ml fluorophore-conjugated phalloidin in 1× phosphate-buffered saline (PBS; 135 mM NaCl, 3.2 mM Na_2HPO_4, 1.3 mM KCl, 0.5 mM

KH_2PO_4, pH 7.4). This was followed by two rinses in Triton-antibody wash (1× PBS, 0.1% bovine serum albumin [BSA], 0.2% TX-100). Blocking was performed by washing samples three times for 10 min each in antibody wash (1× PBS, 0.1% BSA, 0.1% Triton X-100) supplemented with 1 U/ml fluorophore-conjugated phalloidin, followed by washing three times for 10 min each in antibody wash alone. Samples were then processed using standard procedures (Cox and Spradling, 2003) and were mounted in 1 mg/ml phenylenediamine in 50% glycerol, pH 9 (Platt and Michael, 1983), on glass slides.

The following primary antibodies were obtained from the Developmental Studies Hybridoma Bank (DSHB; developed under the auspices of the National Institute of Child Health and Human Development and maintained by the Department of Biology, University of Iowa, Iowa City, IA) and used at the concentrations indicated: mouse anti-Enabled (5G2; Goodman, C.), 1:500; mouse anti-Quail (6B9; Cooley, L.), 1:50; mouse anti–Hts RC (hts RC; Cooley, L.), 1:100; and mouse anti-Gurken (1D12; Schupbach, T.), 1:40. The rabbit anti-Staufen polyclonal antibody (Stau 36; St Johnston *et al.*, 1991), a generous gift from Daniel St. Johnston' s lab, was used at 1:2000. Additional stains used and their concentrations are as follows: rhodamine::phalloidin, 1:500; Alexa Fluor (AF) 488::phalloidin, 1:500; AF647::phalloidin, 1:250 or 1:500; and DAPI (5 mg/ml), 1:10,000 (all from Invitrogen, Carlsbad, CA). The following secondary antibodies were used at 1:1000: AF488::goat anti-mouse, AF568::goat anti-mouse, AF633::goat anti-mouse, AF488::goat anti-rabbit, and AF568::goat anti-rabbit (Invitrogen).

Follicle staging

Follicles were staged based on their morphological appearance as previously described (reviewed in Spradling, 1993). In short, follicles were scored as S8 if they were the right approximate size, were just beginning to elongate in shape (ellipsoid), and exhibited a follicle layer that was completely uniform and composed of cuboidal cells. Follicles were identified as S9 if they had undergone elongation, became ellipsoid in shape, and met the following criteria: 1) the border cells had visibly delaminated from the surrounding epithelia, forming a rosette structure at the anterior of the follicle, and/or 2) the main body follicle cells were in the process of their posterior migration, forming a clear anterior-to-posterior gradient of follicle cell thickness. Follicles in which half of the total follicle length was composed of the oocyte, the main body follicle cells had reached the nurse cell/oocyte boundary, the total follicle length was less than the size of a S14 follicle, and the centripetal follicle cells had not yet begun migrating over the anterior surface of the oocyte were staged as S10A follicles. If half of the total follicle length was composed of the oocyte, the main body follicle cells had reached the nurse cell/oocyte boundary, the follicle length was equal to a S14 follicle, and the centripetal follicle cells had begun to migrate over the anterior surface of the oocyte, the follicle was staged as S10B.

Quantification of early-actin-remodeling defects

S9–S10A follicles were scored as having wild-type morphology, early actin bundle formation, or actin aggregate formation. S10B follicles were scored as having normal actin bundle formation for the given genotype (wild type: well-organized, evenly distributed, and even-length bundles; pxt^{EY}: reduced bundle formation and abnormal distribution and length; pxt^{f}: severe loss of bundle formation), actin bundle formation with actin aggregates, or actin aggregates only. Phenotypic scoring was performed using either a Leica DM IRBE inverted microscope with a PL APO 40×/0.75 ∞/0.17/D objective (506036; Leica Microsystems, Buffalo Grove, IL) or a Nikon Eclipse E600 upright microscope with a Plan Fluor 40×/0.75 ∞/0.17 WD 0.72 objective (Nikon Instruments, Melville, NY). We compared the distributions of actin phenotypes for each genotype and tested for statistical significance using global chi-square tests or Fisher's exact tests using SAS 9.3 (SAS Institute, Cary, NC).

Assessing follicle death

Ovaries were dissected to maintain intact ovarioles and fixed in 4% paraformaldehyde for 10 min at room temperature. Samples were washed five times for 10 min each in antibody wash and stained with DAPI (5 mg/ml), 1:5000, for 30 min at room temperature. Samples were mounted to maintain intact ovarioles in 1 mg/ml phenylenediamine in 50% glycerol, pH 9 (Platt and Michael, 1983). Follicle death was assessed by the presence of condensed and/or fragmented nurse cell nuclei. Ovarioles were scored as having no dying follicles, one or more S8 dying follicles, or one or more ≥S9 dying follicles. Phenotypic scoring was performed using a Nikon Eclipse E600 upright microscope with a Plan Fluor 40×/0.75 ∞/0.17 WD 0.72 objective. We compared the distributions of follicle death for each genotype and tested for statistical significance using global chi-square tests using SAS 9.3.

Confocal microscope image acquisition and processing

All microscopy images were acquired via Zen software on a Zeiss 700 LSM mounted on an Axio Observer.Z1 using a Plan-Apochromat 20×/0.8 M27 or an EC Plan-Apochromat 63×/1.40 Oil DIC M27 objective (Carl Zeiss Microscopy, Thornwood, NY) or via LAS AF SPE Core software on a Leica TCS SPE mounted on a Leica DM2500 using an ACS APO 20×/0.60 IMM CORR-/D or an ACS APO 63×/1.30 Oil CS 0.17/E objective (Leica Microsystems). Maximum projections, image rotation, and cropping were performed in ImageJ (National Institutes of Health, Bethesda, MD; Abramoff *et al.*, 2004). Figure panels were assembled in Illustrator (Adobe, San Jose, CA). To aid in visualization, Figures 1, B–C′ and E–G′; 3, A–F; 5, B–G; 7, A–B″ and D–D″; and 9, A–C‴; and Supplemental Movie S1, A–D, were brightened by 30% using Photoshop (Adobe).

Quantification of Ena localization to early actin structures

Confocal z-series of S9 follicles were acquired at 63× magnification as described. The Ena and F-actin channels were merged and genotypically blinded. The scorers assessed whether the follicle possessed EF, AG, or no early actin structures and then determined whether the follicles with EF or AG exhibited colocalization of Ena puncta with F-actin through qualitative analysis.

Western blot

Whole ovaries, S9 follicles (~30/lane), and S10B follicles (~15/lane) were dissected in room-temperature Grace's insect media (Lonza, Walkersville, MD). Standard Western blotting techniques were used. The following primary antibodies were used at the indicated concentrations: mouse anti–Enabled (5G2; Goodman, C.; obtained from the DSHB), 1:200; rabbit anti–Pxt (affinity-purified polyclonal antibody generated against a synthetic peptide: CQIRQEHGRIDEVVN; GenScript, Piscataway, NJ), 1:5000; and mouse anti–α–tubulin T9026 (Sigma-Aldrich, St. Louis, MO), 1:500. The following secondary antibodies were used: Peroxidase-AffiniPure goat anti–mouse immunoglobulin G (H+L), 1:5000; and Peroxidase-AffiniPure goat anti-rabbit immunoglobulin G (H+L), 1:5000 (Jackson ImmunoResearch Laboratories, West Grove, PA). Blots were developed with SuperSignal West Pico or Femto Chemiluminescent Substrate (Thermo Scientific, Waltham, MA) and imaged using the ChemiDoc-It Imaging System and VisionWorksLS software (UVP,

Upland, CA). Bands were quantified using densitometry analysis in ImageJ (Abramoff *et al*., 2004). Ena levels were assessed using a minimum of three independent biological samples. Statistical significance was determined using a two-sample *t* test with unequal variance in Excel (Microsoft, Redmond, WA).

Quantitative reverse transcriptase PCR

Whole ovaries and S9 follicles were dissected in room-temperature Grace's insect media (Lonza,) and homogenized in TRIzol (Invitrogen). RNA was extracted following manufacturer's protocol, and samples were treated overnight with DNase (RNase-free DNase; Roche, Indianapolis, IN). After quantification, 400 ng of RNA underwent first-strand cDNA synthesis using the iScript cDNA synthesis kit (Bio-Rad, Hercules, CA). Quantitative real-time PCR analysis was performed with the Bio-Rad CFX96 Real-Time System and iQ SYBR Green Supermix following the manufacturer's protocol. Primers for qPCR experiments were designed to span exon–exon junctions against *ena* (forward, 5′-CCTGGAAGTGCTCAGTGGT-3′; reverse, 5′-CCCATGTCCTCCTCATAGCC-3′), *sdhA* (forward, 5′-CAAGGTTGTCGATAGGTCG-3′; reverse, 5′-CTCACAATAGTCATCTGGGC-3′), and *cyp33* (forward, 5′-TGATACCCGAGTTTATGTGTC-3′; reverse, 5′-GGCCATTGAAAGAGTTCCA-3′). Efficiency of each primer set was assessed with a sequence of serial cDNA dilutions (each primer was roughly 100% efficient), and specificity was confirmed by the presence of a single product in end-point melt curve analysis. Fold change in *ena* expression was determined using the $2^{-\Delta\Delta^{Ct}}$ method of quantification against our two reference genes (*sdhA* and *cyp33*). Each cDNA sample was assessed in triplicate for three independent experiments. Statistical significance was determined using a two-sample *t* test with equal variance in Excel.

ACKNOWLEDGMENTS

We thank the Lin and Frank labs for helpful discussion, members of the Tootle lab for helpful discussion and careful review of the manuscript, and the anonymous reviewers for valuable critiques. A.J.S. was previously supported by National Institutes of Health Predoctoral Training Grant in Pharmacological Sciences T32GM067795. X.C. is supported by Iowa Center for Research by Undergraduates Fellowships and National Science Foundation REU. National Science Foundation MCB-1158527 supports the project. Data storage support was provided by the Institute for Clinical and Translational Science, which is funded through the Clinical and Translational Sciences Award supported by the National Center for Research Resources and the National Center for Advancing Translational Sciences, National Institutes of Health, through Grant UL1RR024979.

REFERENCES

Abramoff MD, Magalhaes PJ, Ram SJ (2004). Image processing with ImageJ. Biophoton Int 11, 36–42.

Allaj V, Guo C, Nie D (2013). Non-steroid anti-inflammatory drugs, prostaglandins, and cancer. Cell Biosci 3, 8.

Aszodi A, Pfeifer A, Ahmad M, Glauner M, Zhou XH, Ny L, Andersson KE, Kehrel B, Offermanns S, Fassler R (1999). The vasodilator-stimulated phosphoprotein (VASP) is involved in cGMP- and cAMP-mediated inhibition of agonist-induced platelet aggregation, but is dispensable for smooth muscle function. EMBO J 18, 37–48.

Banan A, Smith GS, Kokoska ER, Miller TA (2000). Role of actin cytoskeleton in prostaglandin-induced protection against ethanol in an intestinal epithelial cell line. J Surg Res 88, 104–113.

Baum B, Li W, Perrimon N (2000). A cyclase-associated protein regulates actin and cell polarity during *Drosophila* oogenesis and in yeast. Curr Biol 10, 964–973.

Bear JE, Gertler FB (2009). Ena/VASP: towards resolving a pointed controversy at the barbed end. J Cell Sci 122, 1947–1953.

Bearer EL, Prakash JM, Li Z (2002). Actin dynamics in platelets. Int Rev Cytol 217, 137–182.

Bearer EL, Prakash JM, Manchester RD, Allen PG (2000). VASP protects actin filaments from gelsolin: an in vitro study with implications for platelet actin reorganizations. Cell Motil Cytoskeleton 47, 351–364.

Birukova AA, Zagranichnaya T, Fu P, Alekseeva E, Chen W, Jacobson JR, Birukov KG (2007). Prostaglandins PGE(2) and PGI(2) promote endothelial barrier enhancement via PKA- and Epac1/Rap1-dependent Rac activation. Exp Cell Res 313, 2504–2520.

Blume C, Benz PM, Walter U, Ha J, Kemp BE, Renne T (2007). AMP-activated protein kinase impairs endothelial actin cytoskeleton assembly by phosphorylating vasodilator-stimulated phosphoprotein. J Biol Chem 282, 4601–4612.

Bos CL, Richel DJ, Ritsema T, Peppelenbosch MP, Versteeg HH (2004). Prostanoids and prostanoid receptors in signal transduction. Int J Biochem Cell Biol 36, 1187–1205.

Bownes M, Hames BD (1978). Genetic analysis of vitellogenesis in *Drosophila* melanogaster: the identification of a temperature-sensitive mutation affecting one of the yolk proteins. J Embryol Exp Morphol 47, 111–120.

Bownes M, Hodson BA (1980). Mutant Fs(1) 1163 of *Drosophila melanogaster* alters yolk protein secretion from the fat-body. Mol Gen Genet 180, 411–418.

Brand AH, Perrimon N (1993). Targeted gene expression as a means of altering cell fates and generating dominant phenotypes. Development 118, 401–415.

Bulin C, Albrecht U, Bode JG, Weber AA, Schror K, Levkau B, Fischer JW (2005). Differential effects of vasodilatory prostaglandins on focal adhesions, cytoskeletal architecture, and migration in human aortic smooth muscle cells. Artertioscler Thromb Vasc Biol 25, 84–89.

Buszczak M, Freeman MR, Carlson JR, Bender M, Cooley L, Segraves WA (1999). Ecdysone response genes govern egg chamber development during mid-oogenesis in *Drosophila*. Development 126, 4581–4589.

Buszczak M, Lu X, Segraves WA, Chang TY, Cooley L (2002). Mutations in the midway gene disrupt a *Drosophila* acyl coenzyme A: diacylglycerol acyltransferase. Genetics 160, 1511–1518.

Butt E, Abel K, Krieger M, Palm D, Hoppe V, Hoppe J, Walter U (1994). cAMP- and cGMP-dependent protein kinase phosphorylation sites of the focal adhesion vasodilator-stimulated phosphoprotein (VASP) in vitro and in intact human platelets. J Biol Chem 269, 14509–14517.

Carney GE, Bender M (2000). The *Drosophila* ecdysone receptor (EcR) gene is required maternally for normal oogenesis. Genetics 154, 1203–1211.

Chao S, Nagoshi RN (1999). Induction of apoptosis in the germline and follicle layer of *Drosophila* egg chambers. Mech Dev 88, 159–172.

Comer AR, Ahern-Djamali SM, Juang JL, Jackson PD, Hoffmann FM (1998). Phosphorylation of Enabled by the *Drosophila* Abelson tyrosine kinase regulates the in vivo function and protein-protein interactions of Enabled. Mol Cell Biol 18, 152–160.

Cooley L, Verheyen E, Ayers K (1992). Chickadee encodes a profilin required for intercellular cytoplasm transport during *Drosophila* oogenesis. Cell 69, 173–184.

Cox RT, Spradling AC (2003). A Balbiani body and the fusome mediate mitochondrial inheritance during *Drosophila* oogenesis. Development 130, 1579–1590.

Dormond O, Bezzi M, Mariotti A, Ruegg C (2002). Prostaglandin E2 promotes integrin alpha Vbeta 3-dependent endothelial cell adhesion, rac-activation, and spreading through cAMP/PKA-dependent signaling. J Biol Chem 277, 45838–45846.

Drummond-Barbosa D, Spradling AC (2001). Stem cells and their progeny respond to nutritional changes during *Drosophila* oogenesis. Dev Biol 231, 265–278.

Frydman HM, Spradling AC (2001). The receptor-like tyrosine phosphatase lar is required for epithelial planar polarity and for axis determination within *Drosophila* ovarian follicles. Development 128, 3209–3220.

Gates J, Nowotarski SH, Yin H, Mahaffey JP, Bridges T, Herrera C, Homem CC, Janody F, Montell DJ, Peifer M (2009). Enabled and Capping protein play important roles in shaping cell behavior during *Drosophila* oogenesis. Dev Biol 333, 90–107.

Gertler FB, Comer AR, Juang JL, Ahern SM, Clark MJ, Liebl EC, Hoffmann FM (1995). Enabled, a dosage-sensitive suppressor of mutations in the *Drosophila* Abl tyrosine kinase, encodes an Abl substrate with SH3 domain-binding properties. Genes Dev 9, 521–533.

Gertler FB, Niebuhr K, Reinhard M, Wehland J, Soriano P (1996). Mena, a relative of VASP and *Drosophila* Enabled, is implicated in the control of microfilament dynamics. Cell 87, 227–239.

Giorgi F, Deri P (1976). Cell death in ovarian chambers of *Drosophila* melanogaster. J Embryol Exp Morphol 35, 521–533.

Groen CM, Spracklen AJ, Fagan TN, Tootle TL (2012). *Drosophila* Fascin is a novel downstream target of prostaglandin signaling during actin remodeling. Mol Biol Cell 23, 4567–4578.
Guild GM, Connelly PS, Shaw MK, Tilney LG (1997). Actin filament cables in *Drosophila* nurse cells are composed of modules that slide passively past one another during dumping. J Cell Biol 138, 783–797.
Gutzeit HO (1986). The role of microfilaments in cytoplasmic streaming in *Drosophila* follicles. J Cell Sci 80, 159–169.
Halbrugge M, Friedrich C, Eigenthaler M, Schanzenbacher P, Walter U (1990). Stoichiometric and reversible phosphorylation of a 46-kDa protein in human platelets in response to cGMP- and cAMP-elevating vasodilators. J Biol Chem 265, 3088–3093.
Hamberg M, Svensson J, Samuelsson B (1975). Thromboxanes: a new group of biologically active compounds derived from prostaglandin endoperoxides. Proc Natl Acad Sci USA 72, 2994–2998.
Hirata M, Hayashi Y, Ushikubi F, Yokota Y, Kageyama R, Nakanishi S, Narumiya S (1991). Cloning and expression of cDNA for a human thromboxane A2 receptor. Nature 349, 617–620.
Horstrup K, Jablonka B, Honig-Liedl P, Just M, Kochsiek K, Walter U (1994). Phosphorylation of focal adhesion vasodilator-stimulated phosphoprotein at Ser157 in intact human platelets correlates with fibrinogen receptor inhibition. Eur J Biochem 225, 21–27.
Hudson AM, Cooley L (2002). Understanding the function of actin-binding proteins through genetic analysis of *Drosophila* oogenesis. Annu Rev Genet 36, 455–488.
Huelsmann S, Ylanne J, Brown NH (2013). Filopodia-like actin cables position nuclei in association with perinuclear actin in *Drosophila* nurse cells. Dev Cell 26, 604–615.
Kawada N, Klein H, Decker K (1992). Eicosanoid-mediated contractility of hepatic stellate cells. Biochem J 285, Pt 2367–371.
Kloeze J (1966). Influence of prostaglandins on platelet adhesiveness and platelet aggregation. In: Prostaglandins: Proceedings of the Second Nobel Symposium, ed. S Bergström and B Samuelsson, New York: Interscience, 241–252.
Lambrechts A, Kwiatkowski AV, Lanier LM, Bear JE, Vandekerckhove J, Ampe C, Gertler FB (2000). cAMP-dependent protein kinase phosphorylation of EVL, a Mena/VASP relative, regulates its interaction with actin and SH3 domains. J Biol Chem 275, 36143–36151.
Lane ME, Kalderon D (1995). Localization and functions of protein kinase A during *Drosophila* oogenesis. Mech Dev 49, 191–200.
Lucas EP, Khanal I, Gaspar P, Fletcher GC, Polesello C, Tapon N, Thompson BJ (2013). The Hippo pathway polarizes the actin cytoskeleton during collective migration of *Drosophila* border cells. J Cell Biol 201, 875–885.
Mahajan-Miklos S, Cooley L (1994a). Intercellular cytoplasm transport during *Drosophila* oogenesis. Dev Biol 165, 336–351.
Mahajan-Miklos S, Cooley L (1994b). The villin-like protein encoded by the *Drosophila* quail gene is required for actin bundle assembly during oogenesis. Cell 78, 291–301.
Martineau LC, McVeigh LI, Jasmin BJ, Kennedy CR (2004). p38 MAP kinase mediates mechanically induced COX-2 and PG EP4 receptor expression in podocytes: implications for the actin cytoskeleton. Am J Physiol. Renal Physiol 286, F693–F701.
Maruoka M, Sato M, Yuan Y, Ichiba M, Fujii R, Ogawa T, Ishida Kitagawa N, Takeya T, Watanabe N (2012). Abi-1-bridged tyrosine phosphorylation of VASP by Abelson kinase impairs association of VASP to focal adhesions and regulates leukaemic cell adhesion. Biochem J 441, 889–899.
Moncada S, Higgs EA, Vane JR (1977). Human arterial and venous tissues generate prostacyclin (prostaglandin x), a potent inhibitor of platelet aggregation. Lancet 1, 18–20.
Montell DJ, Yoon WH, Starz-Gaiano M (2012). Group choreography: mechanisms orchestrating the collective movement of border cells. Nat Rev Mol Cell Biol 13, 631–645.
Neuman-Silberberg FS, Schupbach T (1993). The *Drosophila* dorsoventral patterning gene gurken produces a dorsally localized RNA and encodes a TGF alpha-like protein. Cell 75, 165–174.
Neuman-Silberberg FS, Schupbach T (1996). The *Drosophila* TGF-alpha-like protein Gurken: expression and cellular localization during *Drosophila* oogenesis. Mech Dev 59, 105–113.
Nezis IP, Stravopodis DJ, Papassideri I, Robert-Nicoud M, Margaritis LH (2000). Stage-specific apoptotic patterns during *Drosophila* oogenesis. Eur J Cell Biol 79, 610–620.
Nolte C, Eigenthaler M, Schanzenbacher P, Walter U (1991). Comparison of vasodilatory prostaglandins with respect to cAMP-mediated phosphorylation of a target substrate in intact human platelets. Biochem Pharmacol 42, 253–262.
Peppelenbosch MP, Tertoolen LG, Hage WJ, de Laat SW (1993). Epidermal growth factor-induced actin remodeling is regulated by 5-lipoxygenase and cyclooxygenase products. Cell 74, 565–575.
Peterson JS, Barkett M, McCall K (2003). Stage-specific regulation of caspase activity in *Drosophila* oogenesis. Dev Biol 260, 113–123.
Petrella LN, Smith-Leiker T, Cooley L (2007). The Ovhts polyprotein is cleaved to produce fusome and ring canal proteins required for *Drosophila* oogenesis. Development 134, 703–712.
Petrucci G, De Cristofaro R, Rutella S, Ranelletti FO, Pocaterra D, Lancellotti S, Habib A, Patrono C, Rocca B (2011). Prostaglandin E2 differentially modulates human platelet function through the prostanoid EP2 and EP3 receptors. J Pharmacol Exp Ther 336, 391–402.
Pierce KL, Fujino H, Srinivasan D, Regan JW (1999). Activation of FP prostanoid receptor isoforms leads to Rho-mediated changes in cell morphology and in the cell cytoskeleton. J Biol Chem 274, 35944–35949.
Platt JL, Michael AF (1983). Retardation of fading and enhancement of intensity of immunofluorescence by p-phenylenediamine. J Histochem Cytochem 31, 840–842.
Pollard TD, Borisy GG (2003). Cellular motility driven by assembly and disassembly of actin filaments. Cell 121, 453–465.
Pula G, Krause M (2008). Role of Ena/VASP proteins in homeostasis and disease. Handb Exp Pharmacol 186, 39–65.
Reinhard M, Jarchau T, Walter U (2001). Actin-based motility: stop and go with Ena/VASP proteins. Trends Biochem Sci 26, 243–249.
Robinson DN, Cant K, Cooley L (1994). Morphogenesis of *Drosophila* ovarian ring canals. Development 120, 2015–2025.
Rorth P (1998). Gal4 in the *Drosophila* female germline. Mech Dev 78, 113–118.
Schupbach T, Wieschaus E (1986). Germline autonomy of maternal-effect mutations altering the embryonic body pattern of *Drosophila*. Dev Biol 113, 443–448.
Smith JB, Silver MJ, Ingerman CM, Kocsis JJ (1974). Prostaglandin D2 inhibits the aggregation of human platelets. Thromb Res 5, 291–299.
Smith JP, Haddad EV, Downey JD, Breyer RM, Boutaud O (2010). PGE2 decreases reactivity of human platelets by activating EP2 and EP4. Thromb Res 126, e23–e29.
Speirs CK, Jernigan KK, Kim SH, Cha YI, Lin F, Sepich DS, DuBois RN, Lee E, Solnica-Krezel L (2010). Prostaglandin Gbetagamma signaling stimulates gastrulation movements by limiting cell adhesion through Snai1a stabilization. Development 137, 1327–1337.
Spradling AC (1993). Developmental genetics of oogenesis. In: The Development of *Drosophila melanogaster*, ed. B Martinez-Arias, Cold Spring Harbor, NY: Cold Spring Harbor Laboratory Press, 1–70.
St Johnston D, Beuchle D, Nusslein-Volhard C (1991). Staufen, a gene required to localize maternal RNAs in the *Drosophila* egg. Cell 66, 51–63.
St Johnston D, Brown NH, Gall JG, Jantsch M (1992). A conserved double-stranded RNA-binding domain. Proc Natl Acad Sci USA 89, 10979–10983.
Stanley D, Kim Y (2011). Prostaglandins and their receptors in insect biology. Front Endocrinol (Lausanne) 2, 105.
Tamma G, Wiesner B, Furkert J, Hahm D, Oksche A, Schaefer M, Valenti G, Rosenthal W, Klussmann E (2003). The prostaglandin E2 analogue sulprostone antagonizes vasopressin-induced antidiuresis through activation of Rho. J Cell Sci 116, 3285–3294.
Tani K, Sato S, Sukezane T, Kojima H, Hirose H, Hanafusa H, Shishido T (2003). Abl interactor 1 promotes tyrosine 296 phosphorylation of mammalian enabled (Mena) by c-Abl kinase. J Biol Chem 278, 21685–21692.
Theurkauf WE, Smiley S, Wong ML, Alberts BM (1992). Reorganization of the cytoskeleton during *Drosophila* oogenesis: implications for axis specification and intercellular transport. Development 115, 923–936.
Tootle TL (2013). Genetic insights into the in vivo functions of prostaglandin signaling. Int J Biochem Cell Biol 45, 1629–1632 .
Tootle TL, Spradling AC (2008). *Drosophila* Pxt: a cyclooxygenase-like facilitator of follicle maturation. Development 135, 839–847.
Tootle TL, Williams D, Hubb A, Frederick R, Spradling A (2011). *Drosophila* eggshell production: identification of new genes and coordination by pxt. PLoS One 6, e19943.
Wheatley S, Kulkarni S, Karess R (1995). *Drosophila* nonmuscle myosin II is required for rapid cytoplasmic transport during oogenesis and for axial nuclear migration in early embryos. Development 121, 1937–1946.
Willis AL (1974). An enzymatic mechanism for the antithrombotic and antihemostatic actions of aspirin. Science 183, 325–327.
Yue L, Spradling AC (1992). hu-li tai shao, a gene required for ring canal formation during *Drosophila* oogenesis, encodes a homolog of adducin. Genes Dev 6, 2443–2454.
Yuhki K, Kojima F, Kashiwagi H, Kawabe J, Fujino T, Narumiya S, Ushikubi F (2011). Roles of prostanoids in the pathogenesis of cardiovascular diseases: novel insights from knockout mouse studies. Pharmacol Ther 129, 195–205.